JCI insight

4EBP1-mediated SLC7A11 protein synthesis restrains ferroptosis triggered by MEK inhibitors in advanced ovarian cancer

Jiaxin Yin, … , Ying Xiong, Jing Tan

JCI Insight. 2024. https://doi.org/10.1172/jci.insight.177857.

Research In-Press Preview Oncology Therapeutics

Graphical abstract

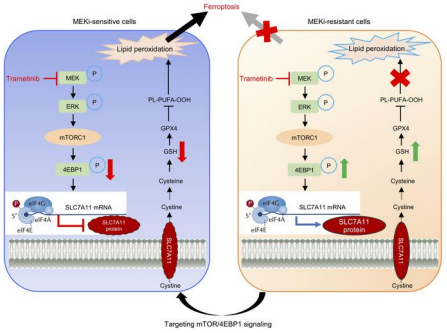

Find the latest version:

https://jci.me/177857/pdf

4EBP1-Mediated SLC7A11 Protein Synthesis Restrains Ferroptosis Triggered by MEK Inhibitors in Advanced Ovarian Cancer

Jiaxin Yin[1], Jianfeng Chen[1#], Jing Han Hong[2], Yulin Huang[1], Rong Xiao[1], Shini Liu[3], Peng Deng[1], Yichen Sun[4], Kelila Xin Ye Chai[5], Xian Zeng[1], Jason Yongsheng Chan[6], Peiyong Guan[8], Yali Wang[1], Peili Wang[1], Chongjie Tong[1], Qiang Yu[2,8], Xiaojun Xia[1], Choon Kiat Ong[2,5,8], Bin Tean Teh[2,7], Ying Xiong[1#] and Jing Tan[1,7,9#]

Affiliations

1. State Key Laboratory of Oncology in South China, Guangdong Provincial Clinical Research Center for Cancer, Sun Yat-sen University Cancer Center, Guangzhou, China.
2. Cancer and Stem Cell Biology Program, Duke-NUS Medical School, Singapore.
3. Department of Oncology, Guangdong Provincial People's Hospital, Guangdong Academy of Medical Sciences, Southern Medical University, Guangzhou, China.
4. Department of Laboratory Medicine, Guangzhou First People's Hospital, School of Medicine, South China University of Technology, Guangzhou, China.
5. Lymphoma Genomic Translational Research Laboratory, Cellular and Molecular Research, National Cancer Centre Singapore, Singapore.
6. Division of Medical Oncology, National Cancer Centre Singapore, Singapore.
7. Laboratory of Cancer Epigenome, Division of Medical Sciences, National Cancer Centre Singapore, Singapore.
8. Genome Institute of Singapore, A*STAR, Singapore.

9. Hainan Academy of Medical Science, Hainan Medical University, Haikou, China.

#Corresponding author:

Dr. Jing Tan

State Key Laboratory of Oncology in South China, Guangdong Provincial Clinical Research Center for Cancer, Sun Yat-sen University Cancer Center, 651 East Dongfeng Road, Guangzhou 510060, PR China; E-mail: tanjing@sysucc.org.cn; Telephone: +86 020-39336156.

Dr. Jianfeng Chen

State Key Laboratory of Oncology in South China, Guangdong Provincial Clinical Research Center for Cancer, Sun Yat-sen University Cancer Center, 651 East Dongfeng Road, Guangzhou 510060, PR China; E-mail: chenjf@sysucc.org.cn; Telephone: +86 020-39336609.

Dr. Ying Xiong

State Key Laboratory of Oncology in South China, Guangdong Provincial Clinical Research Center for Cancer, Sun Yat-sen University Cancer Center, 651 East Dongfeng Road, Guangzhou 510060, PR China; E-mail: xiongying@sysucc.org.cn; Telephone: +86 020-87343871.

Running title

Ferroptosis escape hinders the efficacy of MEK inhibitors in ovarian cancer

Keywords

Ovarian cancer; Ferroptosis; MEK inhibitor; Drug resistance; SLC7A11

Abstract word count: 171

Text word count: 3640

The number of figures: 8

Supplementary files: 1

References: 51

Abstract

Loss of ferroptosis contributes to the development of human cancer, and restoration of ferroptosis has been demonstrated as a potential therapeutic strategy in cancer treatment. However, the mechanisms of how ferroptosis escape contributes to ovarian cancer (OV) development are not well elucidated. Here we show that ferroptosis negative regulation (FNR) signatures correlated with the tumorigenesis of OV and were associated with poor prognosis, suggesting that restoration of ferroptosis represents a potential therapeutic strategy in OV. High throughput drug screening with a kinase inhibitor library identified MEK inhibitors as ferroptosis inducers in OV cells. We further demonstrated that MEK inhibitor resistant OV cells were less vulnerable to trametinib-induced ferroptosis. Mechanistically, mTOR/4EBP1 signaling promoted SLC7A11 protein synthesis, leading to ferroptosis inhibition in MEK inhibitor resistant cells. Dual inhibition of MEK and mTOR/4EBP1 signaling restrained the protein synthesis of SLC7A11 via suppression of the mTOR-4EBP1 activity to reactivate ferroptosis in resistant cells. Together, these findings provide a promising therapeutic option for OV treatment through ferroptosis restoration by the combined inhibition of MEK and mTOR/4EBP1 pathways.

Introduction

Ovarian cancer (OV) has the highest mortality rate among gynecological cancers(1), in part due to its late diagnosis and drug resistance(2). Late-stage diagnoses often lead to drug-resistant forms of the disease, necessitating the need for more effective therapy. Targeted therapies, including VEGF inhibitors and PARP inhibitors, are effective only for a limited number of patients(3). Therefore, it is urgent to explore new therapeutics to improve the clinical outcomes of patients with OV.

Ferroptosis is an iron-dependent form of regulated cell death, caused by excessive lipid peroxidation(4). Among ferroptosis negative regulation (FNR) genes, GPX4 is a core repressor of ferroptosis in cancer cells. It can utilize reduced glutathione (GSH) as a cofactor to detoxify lipid peroxidation, and protect cells against membrane lipid peroxidation(5). Another FNR gene, solute carrier family 7 member 11 (SLC7A11; also known as xCT) works as an amino-acid transporter to uptake extracellular cystine, followed by reduced GSH and eventually inhibition of lipid peroxidation(6). Inhibition of GPX4 and other FNR genes that suppress lipid peroxidation would predispose tumor cells to ferroptosis(5, 7, 8). Conversely, escape of ferroptosis contributes to the development of various tumors such as hepatocellular carcinoma, pancreatic cancer and ovarian cancer(9-11), suggesting that ferroptosis inducers may be potential therapeutic strategies for patients with OV.

Among all the ferroptosis inducers (FINs), erastin is one of the most widely used compounds to trigger ferroptosis in various cancers(8). Nevertheless, due to its limited solubility and low metabolic stability *in vivo*, erastin has been precluded clinically(4).

Meanwhile, several kinase inhibitors have been reported to induce ferroptosis in tumors. For example, sorafenib, the first multi-tyrosine kinase inhibitor approved for patients with hepatocellular carcinoma, was identified as a ferroptosis inducer(12). FGFR4 inhibitors could also trigger ferroptosis in recalcitrant HER2-positive breast cancer and hepatocellular carcinoma(13). Therefore, kinase inhibitors might be effective ferroptosis inducers as potential therapeutic strategies for patients with OV.

Herein, we reported that loss of ferroptosis played a crucial role in the tumorigenesis of OV, and identified MEK inhibitors as potential inducers of ferroptosis. We unraveled a potential mechanism for the escape of ferroptosis triggered by MEK inhibitors, which is through promoting SLC7A11 protein synthesis. We found that targeting mTOR/4EBP1 signaling could restore the ferroptosis by inhibition of SLC7A11 protein synthesis. Therefore, co-targeting both MAPK and mTOR/4EBP1 signaling could provide maximal clinical benefit to patients with OV through inducing ferroptosis.

Results

1. MEK inhibitors trigger ferroptosis in OV.

Ferroptosis-related genes are characterized as ferroptosis positive regulation (FPR) signatures, or FNR signatures in the FerrDb database(14). To determine whether ferroptosis escape plays an important role in OV, we first examined the expression of FNR signatures and glutathione metabolism pathway by TNM plot analysis(15), both of which were found to be significantly upregulated in OV compared to the normal

ovarian tissues (Figure. 1A). The Cancer Genome Atlas (TCGA) and Genotype-Tissue Expression (GTEx) database profiling analysis showed that expressions of ferroptosis suppressors, including SLCA711, GPX4 and FTH1, were also significantly increased in OV compared to the normal ovarian tissues (Figure. 1B). We further confirmed the increased protein level by immunohistochemistry (IHC) analysis in OV tissues. Our analysis showed that high expression of both SLC7A11 and GPX4 was associated with poor patient outcomes (Figure. 1C-1D, Supplementary Figure 1A). These data suggest that loss of ferroptosis is associated with the tumorigenesis and development of OV indicating that reactivation of ferroptosis may be an effective therapeutic option for patients with OV.

To identify novel ferroptosis inducers, we performed a kinase inhibitor library screening with 177 kinase inhibitors in OV cell line A2780. Twenty-six drugs were selected as their inhibition rate of cell viability was more than 20%. We next performed a secondary screening by combining the selected drugs with the ferroptosis inhibitor, Ferrostatin-1 (Fer-1). We identified a total of 15 drugs with a Combo/Fer-1 ratio of more than two as potential ferroptosis inducers (Figure 1E), with erastin used as a positive control of ferroptosis inducer (Supplementary Figure 1B-C). Interestingly, five MEK inhibitors were among these drugs (Figure 1E). To confirm that ferroptosis is the cell death pathway involved, further studies showed that one of MEK inhibitors, trametinib, could remarkably inhibit cell proliferation and the inhibitory effect was significantly rescued by ferroptosis inhibitors, Fer-1 and Liproxstatin-1 (Lipro-1). In contrast, the apoptosis inhibitor Z-VAD-FMK (Z-VAD) and the necroptosis inhibitor

Necrostatin-1 (Necro-1) could only partially rescue the inhibitory effect of trametinib (Figure 1F-1G, Supplementary Figure 1D). We next detected ferroptosis by determining the amount of lipid peroxides in cellular membranes using BODIPY-C11 probe and flow cytometry analysis. The data showed that trametinib significantly induced lipid peroxidation in A2780 and OVCAR5, which could be significantly reversed by Fer-1 and Lipro-1 (Figure 1H). Moreover, trametinib significantly decreased GSH levels which was partially restored by both Fer-1 and Lipro-1 (Figure 1I). We confirmed the above findings with another MEK inhibitor, PD0325901 (Supplementary Figure 1E-1F). Taken together, these findings suggested that MEK inhibitors could induce ferroptosis and offer an alternative therapy for patients with OV.

2. Loss of ferroptosis is associated with the resistance to MEK inhibitors in OV.

To evaluate the effect of MEK inhibitors on inducing ferroptosis in different OV models, we evaluated lipid peroxidation and intracellular GSH levels in a panel of commercial OV cell lines and OV patient-derived cells (PDCs). To validate the sensitivity of trametinib in OV cell lines, we performed cell viability assay of A2780 and its acquired MEKi-resistant cell A2780R. The data showed that A2780 was sensitive to trametinib while A2780R was persistently resistant at the same dosage of trametinib (Supplementary Figure 2A). Furthermore, we performed cell viability assay of 7 commercial OV cell lines and 6 patient-derived primary cells with trametinib treatment. The results showed that OV90, A2780, OVCAR5, POVC1, POVC3, and POVC4 were MEK inhibitor-sensitive while TOV112D, OVCAR3, OVCAR4, SKOV3, POVC18, POVC19 and POVC20 were MEK inhibitor-resistant (Supplementary Figure 2B-2C).

The results above are consistent with our previous study (16). Notably, trametinib could significantly trigger lipid peroxidation and decrease GSH level in both commercial OV cell lines and PDCs that are sensitive to MEK inhibitors. In contrast, trametinib could only slightly or modestly increase lipid ROS and suppress GSH level in resistant cells (Figure 2A-2D). In addition, by comparing the MEK inhibitor-sensitive cell lines A2780 and OVCAR5 with their respective acquired resistant cell lines, A2780R and OVCAR5R, we observed that trametinib only slightly or barely induced lipid peroxidation in the resistant cell lines, while significantly triggering lipid peroxidation in the sensitive cell lines (Figure 2E). Moreover, transmission electron microscopy (TEM) revealed significant differences in the ultrastructural analysis of mitochondria between the MEK inhibitor-sensitive (A2780) and resistant (A2780R) cell lines (Figure 2F). Notably, after treatment with trametinib, A2780 exhibited shrunken mitochondria with elevated membrane density, a hallmark of ferroptosis, while A2780R did not, suggesting that ferroptosis might be triggered only in MEK inhibitor-sensitive cell lines. Collectively, these findings suggested that ferroptosis was more readily triggered in MEK inhibitor-sensitive cell lines and that escape of ferroptosis may contribute to the resistance of OV cells to MEK inhibitors. Therefore, reactivation of ferroptosis may represent a promising strategy to overcome MEK inhibitor resistance in OV.

3. SLC7A11 protein synthesis dictates the sensitivity of OV cells to ferroptosis triggered by MEK inhibitors.

Glutathione is a tripeptide synthesized from cysteine, glutamate, and glycine, with cysteine being the rate-limiting precursor. In most cancer cells, cysteine is acquired

177 through the uptake of extracellular cystine via the amino acid transporter SLC7A11,
178 which is then reduced to cysteine intracellularly, ultimately fueling GSH biosynthesis(6,
179 17-19). GPX4, a glutathione peroxidase, utilizes reduced GSH as a cofactor to suppress
180 lipid peroxidation(5). Since trametinib decreased GSH levels in sensitive cells but not
181 in resistant cell lines, we hypothesize that SLCA711-GPX4 axis was associated with
182 the sensitivity of OV cells to ferroptosis induced MEK inhibitors. We examined the
183 protein levels of SLC7A11 and GPX4, both of which are in the core signaling pathway
184 of ferroptosis, in both MEK inhibitor-sensitive and resistant cells treated with
185 trametinib. Immunoblotting analysis showed that trametinib dramatically suppressed
186 the expression of SLC7A11 in sensitive cells but not in resistant cells, while the level
187 of GPX4 did not change in both sensitive and resistant cells (Figure 3A). Interestingly,
188 mRNA level of *SLC7A11* was not suppressed by trametinib in sensitive cells, as shown
189 by real-time quantitative reverse transcriptase PCR (qRT-PCR) (Figure 3B). Reduction
190 of SLC7A11 protein levels without a corresponding decrease in its mRNA levels
191 implies either increased protein degradation or decreased protein synthesis (or both)
192 may contribute to SLC7A11 suppression upon trametinib treatment in sensitive cells.
193 Treatment with the proteasome inhibitor MG132 did not rescue SLC7A11 protein levels
194 under trametinib treatment (Figure 3C). Therefore, it is less likely that the change in
195 SLC7A11 protein levels in response to trametinib treatment results from altered
196 SLC7A11 protein degradation.

197 We next hypothesized that trametinib would regulate the protein synthesis of
198 SLC7A11. To test this, we used 4 translation reporters, the promoter and different UTR

fragments from *SLC7A11*: SLC7A11-fluc-FL (promoter region, 5′-UTR, and 3′-UTR), SLC7A11-fluc-T1 (promoter region and 5′-UTR), SLC7A11-fluc-T2 (promoter region, 5′-UTR, and nt 1–3846 of 3′-UTR) and SLC7A11-fluc-T3 (promoter region, 5′-UTR, and nt 3827–7859 of 3′-UTR) (20) (Figure 3D). Using luciferase reporter assays, we found that the activity of luciferase reporter SLC7A11-fluc-FL was significantly inhibited by trametinib in A2780, whereas the mRNA level of SLC7A11-fluc-FL was not affected (Figure 3E). Moreover, only the activity of luciferase reporter SLC7A11-fluc-T1, but not that of SLC7A11-fluc-T2 or SLC7A11-fluc-T3, was significantly suppressed in A2780 treated with trametinib (Figure 3F). Our data suggested that trametinib regulated the translation of SLC7A11 protein through the first half of its 5′-UTR (the T1 region) in the sensitive cells. To further functionally validate that constitutive SLC7A11 activation contributed to resistance to ferroptosis induced by MEK inhibitors, SLC7A11 was depleted in A2780R cells using CRISPR-Cas9 method (Figure 3G). SLC7A11 depletion restored trametinib-induced lipid peroxidation and ferroptosis, as demonstrated by colony formation assay, ATP assay, propidium iodide assay, and lipid peroxidation assay (Figure 3H-3J, Supplementary Figure 3A-3C). More importantly, overexpression of SLC7A11 significantly inhibited trametinib-triggered lipid peroxidation and ferroptosis in sensitive cells (Figure 3K-3N, Supplementary Figure 3D-3F). These findings suggested that SLC7A11 dictates the sensitivity of OV cells to ferroptosis induced by MEK inhibitors.

4. mTOR-4EBP1 pathway modulates SLC7A11 protein synthesis to promote ferroptosis escape upon trametinib treatment.

mTOR signaling pathway is associated with protein translation(21-23). The major effects of mTOR on translation are mediated by its phosphorylation of eIF4E binding proteins (4EBPs). Dephosphorylated 4EBPs bind to cap-binding protein eIF4E to interfere with the assembly of the pre-initiation complex(24-26). Phosphorylation of 4EBPs by mTOR releases 4EBPs from eIF4E, thereby allowing 5′-cap-dependent translation initiation(27). To determine whether MEK inhibitors regulate the mTOR-4EBP1 pathway, we examined the activity of mTOR-4EBP1 pathway upon trametinib treatment by immunoblotting analysis. The data showed that trametinib caused a remarkable decrease in 4EBP1 and S6K phosphorylation in sensitive cells while resistant cells maintained persistent 4EBP1 and S6K activation (Figure 4A, Supplementary Figure 4A), which was consistent with decreased SLC7A11 level after trametinib treatment in sensitive cells. We next investigated whether mTOR-4EBP1 axis is involved in trametinib-mediated SLC7A11 inhibition by deleting 4EBP1 from A2780 with shRNA. In contrast to control group shNC, MEK inhibitors did not decrease the expression of SLC7A11 in MEKi-sensitive cell A2780 with 4EBP1 knocked down (Figure 4B). Further luciferase reporter assays manifested that knockdown of 4EBP1 reversed the suppressive effect of trametinib on SLC7A11 translation in A2780 (Figure 4C). These data indicate that trametinib-mediated SLC7A11 inhibition depends on the activity of mTOR-4EBP1 axis.

4EBP1-4A is a non-phosphorylatable mutant of 4EBP1, in which its phosphorylation sites are replaced with alanines (T37, T46, S65, and T70), allowing 4EBP1 to bind to eIF4E constitutively and inhibit cap-dependent translation(28, 29).

Ectopic expression of 4EBP1-4A could suppress the protein level of SLC7A11 in resistant A2780R cells upon trametinib treatment (Figure 4D). Luciferase reporter assays showed that ectopic expression of 4EBP1-4A enhanced the inhibitory effect of trametinib on SLC7A11 translation in A2780R (Figure 4E). These data revealed that mTOR1-4EBP1 modulated SLC7A11 protein synthesis upon trametinib treatment.

To further determine whether 4EBP1 could modulate the sensitivity to ferroptosis induced by trametinib, we conducted shRNA-mediated 4EBP1 depletion. We found that 4EBP1 depletion could impair trametinib sensitivity. 4EBP1-depleted A2780 treated with trametinib resulted in more colonies and higher cell viability, as well as less lipid ROS production (Figure 4F-4H). Moreover, ectopic expression of 4EBP1-4A re-sensitized the resistant A2780R cells to trametinib-induced ferroptosis as evidenced by fewer colony formation, lower cell viability, as well as enhanced of lipid peroxidation (Figure 4I-4K). Together, our findings suggested that sustained mTOR1-4EBP1 activity maintained SLC7A11 translation, mediating ferroptosis escape upon trametinib treatment in OV.

5. Targeting PI3K/mTOR signaling sensitized resistant cells to ferroptosis induced by MEK inhibitors.

To sensitize resistant cells to ferroptosis induced by MEK inhibitors, we sought to explore an approach that targets protein synthesis and induces ferroptosis. Since the PI3K-AKT-mTOR signaling pathway is a key regulator of protein translation(30), we investigated the combination of inhibitors targeting this pathway with trametinib. We found that combined treatment of PI3K/AKT/mTOR inhibitors and trametinib had a

combinatorial effect in suppressing cell proliferation in SKOV3 and A2780R cells (Figure 5A-5B, Supplementary Figure 5A-5B). Further experiments showed that combined treatment of AKT inhibitors and trametinib had a combinatorial effect in inducing cell death and suppressing cell proliferation in both intrinsic- and acquired-resistant cells (Figure 5C-5E, Supplementary Figure 5C). To investigate whether ferroptosis was involved in this effect, we treated SKOV3 and A2780R cells with MK2206 (AKT inhibitor) and trametinib in the presence or absence of ferroptosis rescue agents. We observed that cell proliferation inhibited by the combination of MK2206 and trametinib was partially restored by the ferroptosis inhibitors deferoxamine (DFO), Lipro-1 or Fer-1 (Figure 5F). Moreover, we detected several ferroptotic events, including lipid peroxidation accumulation and GSH depletion in SKOV3 and A2780R cells. Following treatment with the combination of MK2206 and trametinib, lipid ROS accumulation was significantly increased, and this effect was partially impaired by Lipro-1 and Fer-1 (Figure 5G). Meanwhile, GSH levels were significantly reduced by the treatment of MK2206 and trametinib, indicating GSH depletion had occurred (Figure 5H). These results suggested that targeting PI3K/mTOR signaling can sensitize resistant cells to ferroptosis induced by trametinib.

6. Co-targeting AKT and MEK suppresses the protein synthesis of SLC7A11 via inhibition of mTOR-4EBP1 activity.

To investigate whether targeting PI3K/mTOR could sensitize resistant cells to trametinib-induced ferroptosis by suppressing SLC7A11 protein levels, we performed immunoblot analysis and qRT-PCR. As expected, the mRNA level of *SLC7A11* was not

affected under the treatment of AKT inhibitor and trametinib, while the protein level of SLC7A11 was significantly inhibited in both SKOV3 and A2780R (Figure 6A-6B). More importantly, treatment with the proteasome inhibitor MG132 did not restore SLC7A11 protein levels under combination treatment (Figure 6C). The above data suggested that it is more likely that the change in SLC7A11 protein levels in response to co-treatment results from altered SLC7A11 protein synthesis rather than protein degradation.

A previous study has shown that combined inhibition of AKT and MEK kinase can cause the recruitment of 4EBP1 to suppress cap-dependent translation(28). Our data also confirmed that combined inhibition of MEK and AKT inhibited phosphorylation of important downstream mTOR signaling molecules, p70S6K, S6, and 4EBP1 without any effect on mTOR, MEK or ERK phosphorylation in trametinib-resistant OV cells (Figure 6B, Supplementary Figure 6A). In addition, combined treatment of mTOR inhibitor Rapamycin with MEKi could also inhibit phosphorylation of 4EBP1 and consequently suppress SLC7A11 protein level (Supplementary Figure 6B), suggesting that mTOR-4EBP1 activity was associated with the synthesis of SLC7A11. To investigate whether 4EBP1 is involved in the synthesis of SLC7A11 in the combination of MEK and AKT inhibitors, we conducted shRNA-mediated knockdown of 4EBP1 in A2780R and SKOV3. The results showed that compared to shNC group, SLC7A11 was restored by 4EBP1 depletion under the treatment of trametinib and MK2206 (Figure 6D). The above findings suggested that co-targeting AKT and MEK suppressed the protein synthesis of SLC7A11 dependent on 4EBP1. To further functionally test the

309 role of 4EBP1-SLC7A11 axis in regulating ferroptosis caused by MK2206 and
310 trametinib, we first overexpressed SLC7A11 in A2780R by lentivirus infection
311 (Supplementary Figure 6C). The results showed that SLC7A11 ectopic expression
312 significantly impaired the combination effect of colony formation (Figure 6E).
313 Furthermore, overexpression of SLC7A11 obviously reduced lipid peroxidation
314 induced by treatment with MK2206 and trametinib in A2780R (Figure 6F). Likewise,
315 4EBP1 knockdown significantly impaired the combination effect and partially restored
316 the lipid ROS induced by the combination (Figure 6G-H). Collectively, these results
317 indicated that AKT inhibitor MK2206 could restrain the protein synthesis of SLC7A11
318 dependent on 4EBP1 to sensitize resistant cells to trametinib-induced ferroptosis in OV.
319 **7. AKT inhibitor sensitizes OV to MEK inhibitor-mediated ferroptosis *in vivo*.**
320 To investigate the potential of the combination of trametinib and MK2206 *in vivo*, we
321 assessed the efficacy of this combinatorial therapy in xenograft tumor models. In the
322 SKOV3 xenograft model and OV patient–derived xenograft (PDX) model PDX-
323 POVC15, we observed that the combined treatment of trametinib and MK2206 resulted
324 in a significant reduction in tumor growth and tumor weight compared to single drug
325 treatment (Figure 7A-7B and Supplementary Figure 7A). In addition, the combined
326 treatment of trametinib and MK2206 resulted in higher survival rate with a modest
327 change in body weight in the PDX-POVC15 model (Figure 7C and Supplementary
328 Figure 7B). We also detected the levels of ALT, AST, BUN and creatinine in each group.
329 The results showed that there was no significant change in liver and kidney functions,
330 indicating tolerable side effects for the combination treatment in PDX models (Figure

7D). We also performed IHC staining for SLC7A11 and p-4EBP1(Ser65) in xenograft tumor samples. The IHC data showed that the combination of trametinib and MK2206 exhibited a remarkable suppression of SLC7A11 and p-4EBP1 (Figure 7E-7H). Taken together, these findings provided strong evidence that the combination of MEK inhibitor and AKT inhibitor may have a potent anti-tumor effect in OV treatment with tolerable side effects.

Discussion

Despite advances in biological understanding and modern oncologic treatments of OV, it remains the most lethal amongst gynecological malignancies in women, with estimated survival rates of less than 30% in advanced stages(2). Currently, targeted drugs such as PARP1 and VEGF-A inhibitors are used to delay OV progression and improve survival rates, but response rates are typically less than 50% in the relapsed or refractory setting, and acquired drug resistance invariably occurs with prolonged usage (31). Therefore, other drugs that leverage on the other vulnerabilities of OV, such as ferroptosis inducers are being explored(11, 32). In addition, platinum-tolerant OV cells with altered glutathione metabolism that depend on GPX4 for survival have been shown to be highly susceptible to ferroptosis inducers, GPX4 inhibitors(33). Thus, there is an urgent need to explore new therapeutic strategies targeting ferroptosis for OV treatment to improve clinical outcomes.

Targeting the MAPK signaling pathway has been explored across multiple studies in OV. In a recent meta-analysis on the clinical efficacy of monotherapy with a MAPK signaling pathway inhibitor, MEK inhibitors demonstrated a pooled overall response

rate of 20%(34). In this study, we demonstrated the crucial role of FNR signatures in OV tumorigenesis and identified MEK inhibitors as potential inducers of ferroptosis in OV. However, we also found that certain groups of OV that are known to be resistant to MEK inhibitors are less susceptible to trametinib-induced ferroptosis, meaning that not all the OV patients will benefit from the treatment. Therefore, we embarked to mechanistically dissect how MEK inhibitor can induce ferroptosis, with the goal to improve effectiveness of clinical treatment that leverages on the use of MEK inhibitor trametinib. We discovered that in MEK inhibitor resistant OV cells, the protein synthesis of SLC7A11 was upregulated, which mediated the suppression of trametinib-induced ferroptosis. Interestingly, inhibition of mTOR-4EBP1 activity can repress the protein synthesis of SLC7A11 to promote trametinib-induced ferroptosis even in OV cells with resistance to MEK inhibitors (Figure 8), consistent with the roles of mTOR-4EBP1 in mRNA translation(25). The mTOR inhibitor, rapamycin, can decrease GPX4 protein translation at least partially through suppressing the activation of Rag-mTOR-4EBP1 signaling axis(35). Another two studies also show that the synthesis of cyclin D1 and PTEN are regulated by mTOR-driven cap-dependent translation(36, 37). Therefore, therapeutically targeting mTOR/4EBP1/SLC7A11 axis is a viable option to promote trametinib-induced ferroptosis in OV.

The level of SLC7A11 could be regulated through multiple mechanisms, including transcriptional and post-transcriptional levels. For example, SLC7A11 could be transcriptionally upregulated by NRF2(38). Deubiquitinase, such as OTUB1 and DUBA, could deubiquitinate and stabilize SLC7A11 protein to suppress ferroptosis(39,

40). In addition, another study reported that RBMS1 could bind to the eIF3d complex to promote SLC7A11 translation(20). Furthermore, SLC7A11 was found to be transcriptionally regulated by mTORC1 signaling via ATF4(41). In our study, we demonstrated that mTOR signaling promotes SLC7A11 protein synthesis through 4EBP1 activity, whereas targeting mTOR-4EBP1 axis by MEK inhibitor could suppress SLC7A11 protein synthesis to induce ferroptosis.

Combination therapy with PI3K/AKT inhibitors and MAPK/ERK inhibitors has shown promise in preclinical studies by demonstrating synergistic antiproliferative activity in various cancers(42-44). However, combining AKT inhibitors with MEK inhibitors has shown tolerability issues in clinical trials(44, 45). Therefore, design and synthesis of new drugs that can co-target both MAPK and PI3K/AKT, to generate fewer adverse side effects, are critically warranted.

In conclusion, our study identifies a novel function of MEK inhibitors in triggering ferroptosis through suppression of the protein synthesis of SLC7A11. Sustained mTOR/4EBP1/SLC7A11 activity is associated with the resistance to ferroptosis induced by MEK inhibitors, but adding AKT inhibitors can overcome this resistance through inhibiting SLC7A11 protein synthesis. The efficacy of the combination approach has been proven in *in vitro* and *in vivo* OV models. Further investigation is needed to identify more effective therapeutic targets and minimize adverse side effects in the development of small-molecule targeted drugs for patients with OV. Ferroptosis has long been thought to increase the anti-cancer efficacy of immune checkpoint therapies(46, 47). Our proposed combination approach therefore also opens up avenues

to synergize with immunotherapy to achieve greater anti-cancer effects for OV.

Methods

Sex as not a biological variable. These studies included only female animals and patients because ovarian cancer is a disease that only occurs in assigned females at birth.

Cell culture and reagents. All commercial cell lines were purchased from ATCC, except for A2780 (obtained from the European Collection of Authenticated Cell Cultures). No authentication of cell lines was done by the authors. 293T cells were grown in DMEM (Gibco, USA). A2780, OVCAR5, OV90, TOV112D, OVCAR3, OVCAR4, SKOV3, COV504, A2780R and OVCAR5R cells were grown in RPMI-1640 (Gibco). Patient-derived cells were grown in DMEM/F12 (Gibco). Culture medium was supplemented with 10% bovine calf serum (Hyclone, USA) and 1% penicillin/streptomycin (Gibco). Cells were confirmed to be cultured without mycoplasma. All cells were cultivated in 5% CO_2 at 37 ℃. Other reagents were purchased as follows: Trametinib (T2125), MK2206 (T1952), and GSK690693(T6285) were purchased from Target Mol (Shanghai, China). Ferrostatin-1 (S7243), Liproxstatin-1 (S7699), Z-VAD-FMK (S7023), Necrostatin-1 (S8037), MG132 (S2619), PI103 (S1038), BY719 (S2814), Rapamycin (S1039), Everolimus (S1120), erastin (S7242) and kinase inhibitor drug library were purchased from Selleck (Shanghai, China). The drugs above were diluted in DMSO and stored at recommended conditions.

Bioinformatics analysis. FNR genes with score more than two were downloaded from

FerrDb database V2 and analyzed in TNM plot database (https://tnmplot.com/analysis/)(15). Genes of Glutathione metabolism were downloaded from Kyoto Encyclopedia of Genes and Genomes (KEGG) and analyzed in TNM plot database. A web server for cancer and normal gene expression profiling and interactive analyses, GEPIA (http://gepia.cancer-pku.cn/index.html) was recruited to determine the expression of SLC7A11, GPX4 and FTH1 in OV.

Drug screening. A2780 was subjected to a drug screen with a customized kinase inhibitor compound library. Two thousand cells were seeded into a 96-well plate and treated with 186 compounds in the drug screen for 96 hours. Cell viability was assessed using CellTiter-Glo Luminescent Cell Viability Assay (G7570, Promega, USA) according to the product instructions. Inhibitors that resulted in less than 80% cell viability in A2780 were selected for a secondary screen with Ferrostatin-1, a typical ferroptosis inhibitor and drug scoring was calculated by dividing the score of Fer-1/selected drug combination by the single selected drug score. The drugs whose score were more than two were selected as potential ferroptosis inducers. Erastin was a positive control of inducing ferroptosis(48). The result of drug screening is listed in **Supplementary Table 1**.

Cell viability and colony formation assay. 2000 cells were seeded in a 96-well plate for 24 hours and treated with indicated drugs for 96 hours. Cell viability was measured by the CellTiter-Glo Luminescent Cell Viability Assay. Luminescence was detected by a Tecan Infinite M200 Pro plate reader. All conditions were replicated in triplicate. Drug curves were generated using GraphPad Prism 9.0 Software. For colony formation assay,

1×10^4 cells were seeded in a six-well plate and treated with indicated drugs for 9-12 days. The fresh medium was replaced every 3 days. After washed with PBS once, surviving colonies were fixed with methanol for 5 minutes and stained with crystal violet for 5 minutes.

PI staining and apoptosis assay. Cell-cycle analysis was done by propidium iodide (PI) staining (P4864, Sigma-Aldrich, USA) to quantify the sub-G1 population, which can reflect the quantification of cell death. Briefly, 1×10^5 cells were seeded in a 6-well plate and treated with indicated agents for 72 hours. Cells were harvested and fixed with 70% ethanol for at least 4 hours. The cells were then washed with PBS twice and stained with PI at a concentration of 50 mg/mL. For apoptotic assay, apoptotic cells were quantified using the Annexin V–FITC Apoptosis Detection Kit (A211, Vazyme, China) according to the manufacturer's protocol. All experiments were performed in triplicate. Data were acquired and analyzed using Spectral Cell Analyzer SP6800Z (Sony, Japan) and analyzed by using the FlowJo V9 software.

Analysis of lipid peroxidation. Cells were washed once with PBS and incubated with PBS containing 5 μM C11-BODIPY (581/591) (#D3861, Thermo Fisher Scientific, USA) at 37 °C for 30 min in the dark. Cells were then washed, harvested by trypsinization, washed twice with PBS and then resuspended in 500 to 1000 μL fresh PBS. Lipid ROS levels were analyzed by CytoFLEX (Beckman, USA) with fluorescein isothiocyanate (FITC) channel and Texas red channel.

GSH assay. GSH levels were measured using a GSH-Glo Glutathione Assay kit (V6911,

Promega). In brief, cells were seeded at 2000 cells per well in 96-well white-plates. The medium was removed 20 hours later and indicated drugs were added. 48 hours later, the medium was removed and then 100 μl 1× GSH-GLO Reagent was added to each well following incubated for 30 minutes at room temperature. Then, 100 μL reconstituted Luciferin Detection Reagent was added to each well, mixed gently, and shaken slightly at room temperature for 15 minutes. Luminescence was detected by a multifunctional plate reader and normalized by cell viability respectively.

Transmission Electron Microscopy. For ultrastructural analysis of mitochondria, TEM was used to observe ultrastructural of mitochondria. A2780 and A2780R cells were treated with or without trametinib for 48h, and then harvested to be fixed with 2.5% glutaraldehyde in 0.1 M PBS (pH 7.4) at 4°C overnight. Then the samples were washed thrice with 0.1 M PBS and fixed with 1% OsO4 for 2 hours at 4°C. The samples were then dehydrated through an ethanol gradient and subsequently embedded in Spurr's resin. Ultrathin sections were then collected and stained with either uranylacetate or lead citrate and examined using a transmission electron microscope (HT7800 120kv, HITACHI, Japan).

Immunoblot analysis and antibodies. Briefly, cells were harvested and washed with PBS twice. Then cells were lysed using RIPA buffer. Protein concentrations were measured by Bradford assay (#5000205, Bio-Rad, USA). An equal amount of protein was subjected to SDS-PAGE gel with proper concentration and subsequently transferred to the PVDF membrane (Bio-Rad). After blocking in 5% BSA (A1933, Sigma-Aldrich) or 5% milk (#9999, Cell Signaling Technology (CST), USA) for 3

hours and incubation with primary antibodies and secondary antibodies with appropriate concentration, immunoblotting was observed with ECL Western Blotting Detection Reagents (RPN2209, GE Healthcare Life Sciences, UK) in a Bio-Rad ChemiDoc MP imaging system. The primary antibodies used were as follows: SLC7A11 (#12691S, 1:2000) , p-AKT (Ser473) (#4060S, 1:1000), AKT (#4691S, 1:2000), p-mTOR (#5536S, 1:1000), mTOR (#2983S, 1:1000), p-ERK1/2 (#4370S, 1:2000), ERK1/2 (#4696S, 1:2000), p-MEK (#9154S, 1:1000), MEK (#9126S, 1:1000),β-actin (#3700S, 1:2000), p-P70S6K (Thr389) (#9205S, 1:1000), P70S6K (#9202S, 1:1000), p-S6 (Ser235/236) (#4858S, 1:1000), S6 (#2317S, 1:1000), p-4EBP1 (Ser65) (#9451S, 1:1000) and 4EBP1 (#9644S, 1:1000) were obtained from CST. GPX4 (ab125066, 1:2000) and the anti-rabbit secondary antibody (ab205718, 1:20000) were purchased from Abcam (UK). The anti-mouse secondary antibody (#NA931, 1:5000) was purchased from GE Healthcare Life Sciences.

qRT-PCR. Total RNA was extracted using the RNeasy Mini Kit (74106, Qiagen, Germany); cDNA was subsequently produced using TranScript All-in-One First-Strand cDNA Synthesis SuperMix for RT-PCR (One-Step gDNA Removal) (TransGen Biotech, China). qRT-PCR was conducted following the instructions of PerfectStart Green qPCR SuperMix (TransGen Biotech). 18S was used as an endogenous housekeeping gene for normalization. The primer pairs of the genes used for quantitative qRT-PCR are as follow: SLC7A11 5’-ATGCAGTGGCAGTGACCTTT-3’ and 5’-GGCAACAAAGATCGGAACTG-3’;

18S 5’-GTAACCCGTTGAACCCCATT-3’ and 5’-CCATCCAATCGGTAGTAGCG-

3’; Firefly-luc 5’-GGTACTGTTGGTAAAGCCAC-3’ and 5’-CTCTTCATAGCCTTATGCAG-3’; Renilla-luc 5’-CACTGGGCAGGTGTCCACTC-3’ and 5’-GTTCTGGATCATAAACTTTC-3’. The mRNA levels of these genes were determined as the mean of the Ct values obtained from the couple of primers. Data are described as relative mRNA expression levels.

Plasmid construction and virus infection. SLC7A11-knockdown cell lines were generated using CRISPR/Cas9 technology. To be described, for SLC7A11 gene knockdown, sgRNA sequences were designed using the Optimized CRISPR Design (http://chopchop.cbu. ib.no/) and inserted into the lentiCRISPR v2 vector (#52961, Addgene, USA) containing the Streptococcus pyogenes Cas9 nuclease gene. Guide RNA sequences targeting the SLC7A11 are as follows. SLC7A11 sgRNA#1: 5’ CACCGACCATAGTAGGGACACACGG 3’ and 5’ AAACCCGTGTGTCCCTACTATGGTC 3’; SLC7A11 sgRNA#2: 5’ CACCGTATGGGACAAGAAACCCAGG 3’ and 5’ AAACCCTGGGTTTCTTGTCCCATAC 3’. ShRNA sequences targeting human 4EBP1 (TRCN 0000040203, Sigma-Aldrich) were cloned into PLKO.1 plasmid (#10878, Addgene) and the knockdown effect of shRNA sequences targeting human 4EBP1 have been validated in previous studies(49, 50). The plasmids of pCDH-EF1-Neo-SLC7A11-myc and pCDH-EF1-Neo were gifts from Dr. Zhu Xiaofeng, coming from Sun Yat-sen University Cancer Center in Guangzhou of China. Human 4EBP1 was amplified from HEK293T cDNA and then cloned into the pCDH-CMV-MCS-EF1-copGFP-T2A-Puro lentiviral expression vector (System Biosciences, USA) to obtain

pCDH-4EBP1 plasmid. Then we generated the mutant of pCDH-4EBP1 by using the KOD -Plus- Mutagenesis kit (SMK-101, TOYOBO, Japan) to obtain pCDH-4EBP1-4A plasmid (containing four mutation sites, including T37A, T46A, S65A, T70A).

The lentiviral vectors were transfected into HEK293T packaging cells with Lipofectamine 2000 (#11668019, Thermo Fisher Scientific). The viral supernatants were passed through a 0.45 μm nitrocellulose filter and were used to infect target cells. After transfected for 48 hours, stably transfected cells were selected with 1.0 μg/mL puromycin (Sigma-Aldrich) for 4 days or 1mg/mL G-418 disulfate (T6512, Target Mol) for one week.

Luciferase reporter assay. The plasmids of SLC7A11-FL, SLC7A11-T1, SLC7A11-T2 and SLC7A11-T3 are gifts from Dr. Wang Yang at Dalian Medical University in Dalian of China and have been described in previous study (20). Luciferase reporter assay was performed using a Dual-Luciferase Reporter Assay System (E1910, Promega) according to the product instructions. Briefly, 3×10^5 targeted cells seeded in 12 well-plates were transfected with 1 μg targeted plasmids and 100 ng pRL-TK for 48 h. The cells were washed once with PBS and 100 ul lysis buffer each well was added to lyse cells for one hour at room temperature. Then extract 20ul supernatant and split into 96-well white-plate for subsequent luciferase activity measurement, following product instructions. Luminescence from three independent samples was recorded using a multifunctional plate reader.

Mouse xenograft experiment. The 6-week-old female nude mice used in this study were purchased from Beijing Vital River Laboratory Animal Technology Co (Beijing,

549 China). Tumor size and body weight was measured twice to three times a week, and
550 volume of tumor was calculated with the formula: $width^2 \times length \times 0.537$, length
551 represents the longest diameter and width means the shortest diameter.

552 For the SKOV3 tumor xenograft experiment, 4×10^6 SKOV3 cells were injected
553 subcutaneously in the right flank of the BALB/c nude mice. For PDX mouse models,
554 PDX-POVC15 tumor masses were performed to passage into NOD/SCID mice. When
555 the tumors reached approximately 100 mm^3, the mice were randomly divided into 4
556 groups for treatment: (a) vehicle; (b)trametinib; (c) MK2206; and (d) combination
557 (trametinib and MK2206). Trametinib was dissolved in 0.5% methylcellulose and 0.2%
558 Tween-80, and MK2206 was prepared in PBS containing 30% captisol. Drug dosages
559 were given as follows: trametinib, 0.25 mg/kg every other day (intraperitoneal
560 injection); MK2206, 60 mg/kg in SKOV3 and 90 mg/kg in PDX-POVC15 every other
561 day (orally). When tumor volume of the vehicle group reached about 1000mm^3, mice
562 were sacrificed using CO_2 and tumors were collected for further analysis.

563 For animal survival study, PDX-POVC15 tumor masses were performed to passage
564 into NOD/SCID mice. When the tumors reached approximately 100 mm^3, the mice
565 were randomly divided into 4 groups to receive therapy as described in xenograft
566 experiments. Drug treatment was withdrawn until the tumor volume of the first mouse
567 reached 1000 mm^3. Animal survival of every mouse was evaluated from the first day
568 of treatment until the tumor volume reached 1000 mm^3, following detecting the levels
569 of alanine aminotransferase (ALT), aspartate aminotransferase (AST), BUN and
570 creatinine in the serum of PDX-POVC15.

IHC staining. IHC staining was conducted using standard procedures. Xenograft tumors were harvested, fixed with 10% formalin immediately, and embedded in paraffin. After deparaffinization, rehydration, antigen retrieval by heat-induced epitope retrieval, endogenous peroxidase was blocked with 3% H_2O_2 at room temperature. Antibodies specific to SLC7A11 (1:100; 12691S, CST), p-4EBP1(1:800,2855S, CST) and GPX4 (1:500, 52455S, CST) were used in this study and tissues were incubated overnight at 4°C. On the second day, after incubation of secondary antibodies (Dako REAL HRP Rabbit detection kit, Denmark) for 30 minutes, the DAB reagent kit (ZLI-9019, ZSGB-BIO, China) was used as chromogen and hematoxylin (ZLI-9609, ZSGB-BIO) was used as counterstain. Histoscore was a multiplicative index of the intensity of staining and the proportion of positive tumor cells. The intensity was graded as follows: 0, negative staining; 1, mild staining; 2, moderate staining; 3, strong staining. The percentage of stained cells was defined as follows: 1, less than 10%; 2, 10%–50%; 3, 50%–75%; 4, more than 75%.

For human ovarian cancer tissues analysis, the optimal cutoff point of SLC7A11 expression was performed based on X-tile software (X-tile 3.6.1) (51) ,which was used to classify tumors into high expression group and low expression group. In this study, SLC7A11 histoscore with 0~3 was identified as SLC7A11 low expression (24 cases) while histoscore with 4~12 was considered as SLC7A11 high expression (20 cases). GPX4 histoscore with 0~4 was identified as GPX4 low expression (17 cases) while histoscore with 5~12 was considered as GPX4 high expression (27 cases).

Statistical analysis. Comparisons between two groups were analyzed by two-tailed

Student's t tests with GraphPad Prism 9.0 Software. Comparisons among more than two groups were analyzed using 1-way ANOVA. Survival curves were described by Kaplan-Meier plots and compared with the log-rank test. 2-way ANOVA was used to calculate differences between two curves with multiple time or concentration points. Data are presented as mean ± SD unless otherwise stated, with at least three biological replicates in each group. P values less than 0.05 were considered statistically significant.

Study approval. All procedures of animal work were performed in compliance with standard procedures approved by the Institutional Animal Care and Use Committee of Sun Yat-sen University. We have obtained all human material approved by the medical ethics committee of the Sun Yat-sen University Cancer Center and signed patient informed consent.

Data availability

The key raw data are available at Research Data Deposit public platform (www.researchdata.org.cn) with approval number RDDB2024608391. The relevant reagents such as plasmids are available from the corresponding authors upon request. Values for all data points in graphs are reported in the supplemental **Supporting Data Values file**.

Conflict of Interest

The authors declare no conflict of interest.

Author Contribution Statement

J. Y. and J. T. designed and conceived the study. J. Y. conducted the most experiments

and prepared the manuscript. J. T. supervised the project. J. T., Y.X. and J.C. revised the manuscript. Y. H., X. Z., R. X. and J.C. contributed to the technical support and animal work. P. D., S.L., Y. S., P.W., Y.W., C.T. and J. G. provided material support. J.H.H., J.Y.C., P.G, K.X.C, B.T.T., Q.Y., Y.X., X.X. and C.K.O provided a critical reading of the manuscript. All the authors have given their consent to publish this study.

Acknowledgements

We appreciate Dr. Wang Yang for the gifts of SLC7A11 relative luciferase reporter plasmids. We appreciate that Dr. Zhu Xiaofeng provided us with the human SLC7A11 plasmid. We also thank all the patients who donated samples for this study. This work was supported by the National Natural Science Foundation of P. R. China (82320108015, 82073391 and 82170188), National Key Research and Development Program of China (No. 2022YFA1304000), and Guangzhou Science and Technology Program (2023B01J1004).

References

1. Siegel RL, Miller KD, Wagle NS, and Jemal A. Cancer statistics, 2023. *CA Cancer J Clin.* 2023;73(1):17-48.
2. Lheureux S, Gourley C, Vergote I, and Oza AM. Epithelial ovarian cancer. *Lancet.* 2019;393(10177):1240-53.
3. Lheureux S, Braunstein M, and Oza AM. Epithelial ovarian cancer: Evolution of management in the era of precision medicine. *CA Cancer J Clin.* 2019;69(4):280-304.

4. Dixon SJ, Lemberg KM, Lamprecht MR, Skouta R, Zaitsev EM, Gleason CE, et al. Ferroptosis: an iron-dependent form of nonapoptotic cell death. *Cell.* 2012;149(5):1060-72.
5. Yang WS, SriRamaratnam R, Welsch ME, Shimada K, Skouta R, Viswanathan VS, et al. Regulation of ferroptotic cancer cell death by GPX4. *Cell.* 2014;156(1-2):317-31.
6. Sato H, Tamba M, Ishii T, and Bannai S. Cloning and expression of a plasma membrane cystine/glutamate exchange transporter composed of two distinct proteins. *J Biol Chem.* 1999;274(17):11455-8.
7. Dixon SJ, Patel DN, Welsch M, Skouta R, Lee ED, Hayano M, et al. Pharmacological inhibition of cystine-glutamate exchange induces endoplasmic reticulum stress and ferroptosis. *eLife.* 2014;3:e02523.
8. Lei G, Zhuang L, and Gan B. Targeting ferroptosis as a vulnerability in cancer. *Nature Reviews Cancer.* 2022;22(7):381-96.
9. Yao F, Deng Y, Zhao Y, Mei Y, Zhang Y, Liu X, et al. A targetable LIFR-NF-kappaB-LCN2 axis controls liver tumorigenesis and vulnerability to ferroptosis. *Nat Commun.* 2021;12(1):7333.
10. He F, Zhang P, Liu J, Wang R, Kaufman RJ, Yaden BC, et al. ATF4 suppresses hepatocarcinogenesis by inducing SLC7A11 (xCT) to block stress-related ferroptosis. *Journal of hepatology.* 2023;79(2):362-77.
11. Wang CK, Chen TJ, Tan GYT, Chang FP, Sridharan S, Yu CA, et al. MEX3A Mediates p53 Degradation to Suppress Ferroptosis and Facilitate Ovarian Cancer Tumorigenesis. *Cancer Res.* 2023;83(2):251-63.
12. Louandre C, Ezzoukhry Z, Godin C, Barbare JC, Mazière JC, Chauffert B, et al. Iron-dependent cell death of hepatocellular carcinoma cells exposed to sorafenib. *International journal of cancer.* 2013;133(7):1732-42.
13. Zou Y, Zheng S, Xie X, Ye F, Hu X, Tian Z, et al. N6-methyladenosine regulated FGFR4 attenuates ferroptotic cell death in recalcitrant HER2-positive breast cancer. *Nat Commun.* 2022;13(1):2672.
14. Zhou N, Yuan X, Du Q, Zhang Z, Shi X, Bao J, et al. FerrDb V2: update of the manually curated database of ferroptosis regulators and ferroptosis-disease associations. *Nucleic acids research.* 2023;51(D1):D571-D82.
15. Bartha A, and Gyorffy B. TNMplot.com: A Web Tool for the Comparison of Gene Expression in Normal, Tumor and Metastatic Tissues. *International journal of molecular sciences.* 2021;22(5).
16. Liu S, Zou Q, Chen JP, Yao X, Guan P, Liang W, et al. Targeting enhancer reprogramming to mitigate MEK inhibitor resistance in preclinical models of advanced ovarian cancer. *J Clin Invest.* 2021;131(20).
17. Conrad M, and Sato H. The oxidative stress-inducible cystine/glutamate antiporter, system x (c) (-) : cystine supplier and beyond. *Amino Acids.* 2012;42(1):231-46.
18. Koppula P, Zhang Y, Zhuang L, and Gan B. Amino acid transporter SLC7A11/xCT at the crossroads of regulating redox homeostasis and nutrient dependency of cancer. *Cancer Commun (Lond).* 2018;38(1):12.
19. Liu X, Olszewski K, Zhang Y, Lim EW, Shi J, Zhang X, et al. Cystine transporter regulation of pentose phosphate pathway dependency and disulfide stress exposes a targetable metabolic vulnerability in cancer. *Nat Cell Biol.* 2020;22(4):476-86.
20. Zhang W, Sun Y, Bai L, Zhi L, Yang Y, Zhao Q, et al. RBMS1 regulates lung cancer ferroptosis

through translational control of SLC7A11. *J Clin Invest.* 2021;131(22).
21. Bhat M, Robichaud N, Hulea L, Sonenberg N, Pelletier J, and Topisirovic I. Targeting the translation machinery in cancer. *Nat Rev Drug Discov.* 2015;14(4):261-78.
22. Saxton RA, and Sabatini DM. mTOR Signaling in Growth, Metabolism, and Disease. *Cell.* 2017;169(2):361-71.
23. Liu GY, and Sabatini DM. mTOR at the nexus of nutrition, growth, ageing and disease. *Nat Rev Mol Cell Biol.* 2020;21(4):183-203.
24. Fabbri L, Chakraborty A, Robert C, and Vagner S. The plasticity of mRNA translation during cancer progression and therapy resistance. *Nat Rev Cancer.* 2021;21(9):558-77.
25. Gingras AC, Gygi SP, Raught B, Polakiewicz RD, Abraham RT, Hoekstra MF, et al. Regulation of 4E-BP1 phosphorylation: a novel two-step mechanism. *Genes Dev.* 1999;13(11):1422-37.
26. Sonenberg N, and Hinnebusch AG. Regulation of translation initiation in eukaryotes: mechanisms and biological targets. *Cell.* 2009;136(4):731-45.
27. Siddiqui N, and Sonenberg N. Signalling to eIF4E in cancer. *Biochem Soc Trans.* 2015;43(5):763-72.
28. She QB, Halilovic E, Ye Q, Zhen W, Shirasawa S, Sasazuki T, et al. 4E-BP1 is a key effector of the oncogenic activation of the AKT and ERK signaling pathways that integrates their function in tumors. *Cancer Cell.* 2010;18(1):39-51.
29. Cai W, Ye Q, and She QB. Loss of 4E-BP1 function induces EMT and promotes cancer cell migration and invasion via cap-dependent translational activation of snail. *Oncotarget.* 2014;5(15):6015-27.
30. Lee BJ, Boyer JA, Burnett GL, Thottumkara AP, Tibrewal N, Wilson SL, et al. Selective inhibitors of mTORC1 activate 4EBP1 and suppress tumor growth. *Nat Chem Biol.* 2021;17(10):1065-74.
31. Tendulkar S, and Dodamani S. Chemoresistance in Ovarian Cancer: Prospects for New Drugs. *Anticancer Agents Med Chem.* 2021;21(6):668-78.
32. You Y, Fan Q, Huang J, Wu Y, Lin H, and Zhang Q. Ferroptosis-Related Gene Signature Promotes Ovarian Cancer by Influencing Immune Infiltration and Invasion. *J Oncol.* 2021;2021(1687-8450 (Print)):9915312.
33. Wang Y, Zhao G, Condello S, Huang H, Cardenas H, Tanner EJ, et al. Frizzled-7 Identifies Platinum-Tolerant Ovarian Cancer Cells Susceptible to Ferroptosis. *Cancer Res.* 2021;81(2):384-99.
34. Hendrikse CSE, Theelen PMM, van der Ploeg P, Westgeest HM, Boere IA, Thijs AMJ, et al. The potential of RAS/RAF/MEK/ERK (MAPK) signaling pathway inhibitors in ovarian cancer: A systematic review and meta-analysis. *Gynecol Oncol.* 2023;171:83-94.
35. Liu Y, Wang Y, Liu J, Kang R, and Tang D. Interplay between MTOR and GPX4 signaling modulates autophagy-dependent ferroptotic cancer cell death. *Cancer Gene Ther.* 2021;28(1-2):55-63.
36. Mukherjee R, Vanaja KG, Boyer JA, Gadal S, Solomon H, Chandarlapaty S, et al. Regulation of PTEN translation by PI3K signaling maintains pathway homeostasis. *Mol Cell.* 2021;81(4):708-23 e5.
37. Cowling VH. Enhanced mRNA cap methylation increases cyclin D1 expression and promotes cell transformation. *Oncogene.* 2010;29(6):930-6.
38. Sayin VI, LeBoeuf SE, Singh SX, Davidson SM, Biancur D, Guzelhan BS, et al. Activation of

the NRF2 antioxidant program generates an imbalance in central carbon metabolism in cancer. *eLife.* 2017;6.

39. Liu T, Jiang L, Tavana O, and Gu W. The Deubiquitylase OTUB1 Mediates Ferroptosis via Stabilization of SLC7A11. *Cancer Research.* 2019;79(8):1913-24.

40. Wang ZL, Ouyang LL, Liu N, Li TS, Yan BK, Mao C, et al. The DUBA-SLC7A11-c-Myc axis is critical for stemness and ferroptosis. *Oncogene.* 2023;42(36):2688-700.

41. Torrence ME, MacArthur MR, Hosios AM, Valvezan AJ, Asara JM, Mitchell JR, et al. The mTORC1-mediated activation of ATF4 promotes protein and glutathione synthesis downstream of growth signals. *eLife.* 2021;10.

42. Weisner J, Landel I, Reintjes C, Uhlenbrock N, Trajkovic-Arsic M, Dienstbier N, et al. Preclinical Efficacy of Covalent-Allosteric AKT Inhibitor Borussertib in Combination with Trametinib in KRAS-Mutant Pancreatic and Colorectal Cancer. *Cancer Res.* 2019;79(9):2367-78.

43. Jokinen E, and Koivunen JP. MEK and PI3K inhibition in solid tumors: rationale and evidence to date. *Ther Adv Med Oncol.* 2015;7(3):170-80.

44. Tolcher AW, Peng W, and Calvo E. Rational Approaches for Combination Therapy Strategies Targeting the MAP Kinase Pathway in Solid Tumors. *Mol Cancer Ther.* 2018;17(1):3-16.

45. Tolcher AW, Patnaik A, Papadopoulos KP, Rasco DW, Becerra CR, Allred AJ, et al. Phase I study of the MEK inhibitor trametinib in combination with the AKT inhibitor afuresertib in patients with solid tumors and multiple myeloma. *Cancer Chemother Pharmacol.* 2015;75(1):183-9.

46. Chung CH, Lin CY, Chen CY, Hsueh CW, Chang YW, Wang CC, et al. Ferroptosis Signature Shapes the Immune Profiles to Enhance the Response to Immune Checkpoint Inhibitors in Head and Neck Cancer. *Advanced science (Weinheim, Baden-Wurttemberg, Germany).* 2023;10(15):e2204514.

47. Wang W, Green M, Choi JE, Gijón M, Kennedy PD, Johnson JK, et al. CD8(+) T cells regulate tumour ferroptosis during cancer immunotherapy. *Nature.* 2019;569(7755):270-4.

48. Fang Y, Tan Q, Zhou H, Xu J, and Gu Q. Discovery and optimization of 2-(trifluoromethyl)benzimidazole derivatives as novel ferroptosis inducers in vitro and in vivo. *European journal of medicinal chemistry.* 2023;245(Pt 1):114905.

49. Hsu HS, Lin MH, Jang YH, Kuo TT, Liu CC, and Cheng TH. The 4E-BP1/eIF4E ratio is a determinant for rapamycin response in esophageal cancer cells. *The Journal of thoracic and cardiovascular surgery.* 2015;149(1):378-85.

50. Githaka JM, Tripathi N, Kirschenman R, Patel N, Pandya V, Kramer DA, et al. BAD regulates mammary gland morphogenesis by 4E-BP1-mediated control of localized translation in mouse and human models. *Nat Commun.* 2021;12(1):2939.

51. Camp RL, Dolled-Filhart M, and Rimm DL. X-tile: a new bio-informatics tool for biomarker assessment and outcome-based cut-point optimization. *Clin Cancer Res.* 2004;10(21):7252-9.

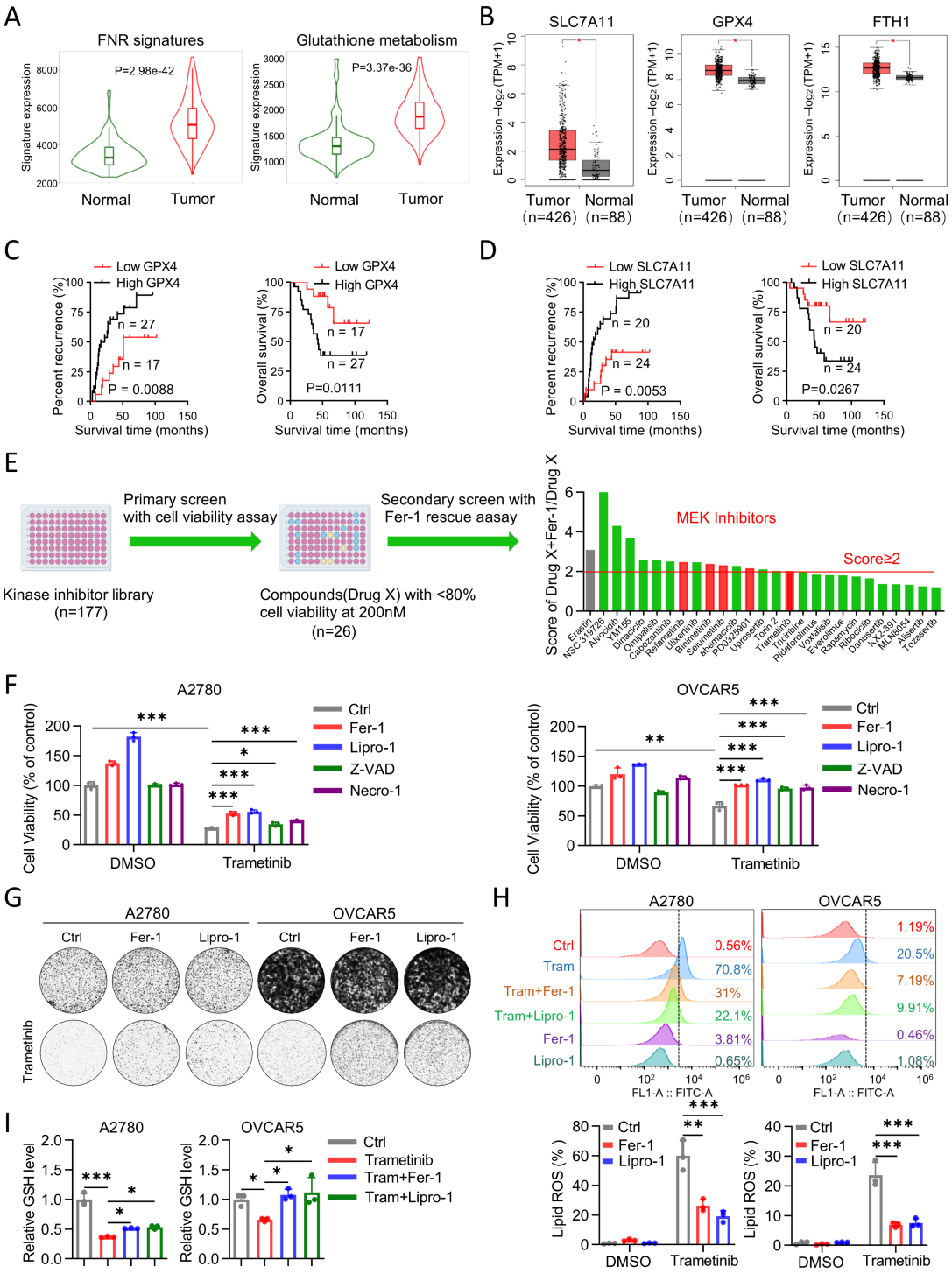
A
FNR signatures
Glutathione metabolism
P=2.98e-42
P=3.37e-36
Signature expression
Normal
Tumor
B
SLC7A11
GPX4
FTH1
Expression –log2 (TPM+1)
Tumor (n=426)
Normal (n=88)
C
Low GPX4
High GPX4
Percent recurrence (%)
Overall survival (%)
n = 27
n = 17
P = 0.0088
P=0.0111
Survival time (months)
D
Low SLC7A11
High SLC7A11
n = 20
n = 24
P = 0.0053
P=0.0267
E
Primary screen with cell viability assay
Secondary screen with Fer-1 rescue aasay
Kinase inhibitor library (n=177)
Compounds(Drug X) with <80% cell viability at 200nM (n=26)
Score of Drug X+Fer-1/Drug X
MEK Inhibitors
Score≥2
Erastin
NSC 319726
Alvocidib
YM155
Dinaciclib
Omipalisib
Cabozantinib
Refametinib
Ulixertinib
Binimetinib
Selumetinib
abemaciclib
PD0325901
Uprosertib
Trametinib
Trifluoperazine
Rolapitamus
Voxtalisib
Everolimus
Rapamycin
Ribociclib
Damnacanthal
KX2-391
MLN8054
Alisertib
Tozasertib
F
A2780
OVCAR5
Cell Viability (% of control)
Ctrl
Fer-1
Lipro-1
Z-VAD
Necro-1
DMSO
Trametinib
G
A2780
OVCAR5
Ctrl
Fer-1
Lipro-1
Trametinib
H
A2780
OVCAR5
Ctrl
Tram
Tram+Fer-1
Tram+Lipro-1
Fer-1
Lipro-1
0.56%
70.8%
31%
22.1%
3.81%
0.65%
1.19%
20.5%
7.19%
9.91%
0.46%
1.08%
FL1-A :: FITC-A
Lipid ROS (%)
I
A2780
OVCAR5
Relative GSH level
Ctrl
Trametinib
Tram+Fer-1
Tram+Lipro-1

Figure 1. MEK inhibitors trigger ferroptosis in OV. (A) Gene expression levels of FNR signatures and Glutathione metabolism pathway in OV tumor and normal tissues analyzed in TNM plot database. **(B)** Gene expression level of GPX4, SLC7A11 and FTH1 in TCGA OV tumor (n = 426) and matched TCGA normal OV tissues along with GTEx data (n = 88). **(C)** Kaplan-Meier curves of recurrence time and overall survival rates in patients with OV grouped according to high (black, n = 17) and low (red, n = 27) expression of GPX4 (log-rank test). **(D)** Kaplan-Meier curves of recurrence time and overall survival rates in patients with OV grouped according to high (black, n = 20) and low (red, n = 24) expression of SLC7A11 (log-rank test). **(E)** The screening process for discovering ferroptosis inducers by performing kinase inhibitors library screening with 177 compounds with the concentration of 200 nM in A2780. **(F)** Cell viability assay of A2780 and OVCAR5 cells treated with vehicle (DMSO) or trametinib (200nM in A2780 and 500 nM in OVCAR5) in the absence or presence of Ferrostatin-1 (Fer-1) (2μM), Liproxstatin-1 (Lipro-1) (100nM), Necrostatin-1 (Necro-1) (5μM) and Z-VAD-FMK (Z-VAD) (5μM) for 72 hours. **(G)** Colony formation assay in A2780 and OVCAR5 treated with vehicle (DMSO) or the trametinib (100 nM in A2780 and 200 nM in OVCAR5) in the absence or presence of Fer-1 (2μM) and Lipro-1 (100nM). **(H)** Lipid peroxidation assay of A2780 and OVCAR5 cells treated with trametinib (200nM in A2780 and 500 nM in OVCAR5) combined with or without Fer-1 or Lipro-1 for 48 hours. Lipid peroxidation was assessed by using BODIPY™ 581/591 C11 staining followed by FACS analysis. **(I)** Intracellular GSH level of A2780 and OVCAR5 cells treated with trametinib (200nM in A2780 and 500 nM in OVCAR5) with or without Lipro-1 (100nM) for 48 hours. (C and D) P-values were determined by log-rank test. (F, H and I) Results are represented as mean ± SD of 3 biological replicates. P-values were determined by 1-way ANOVA with Bonferroni's post hoc test. $*P < 0.05$, $**P < 0.01$, $***P < 0.001$.

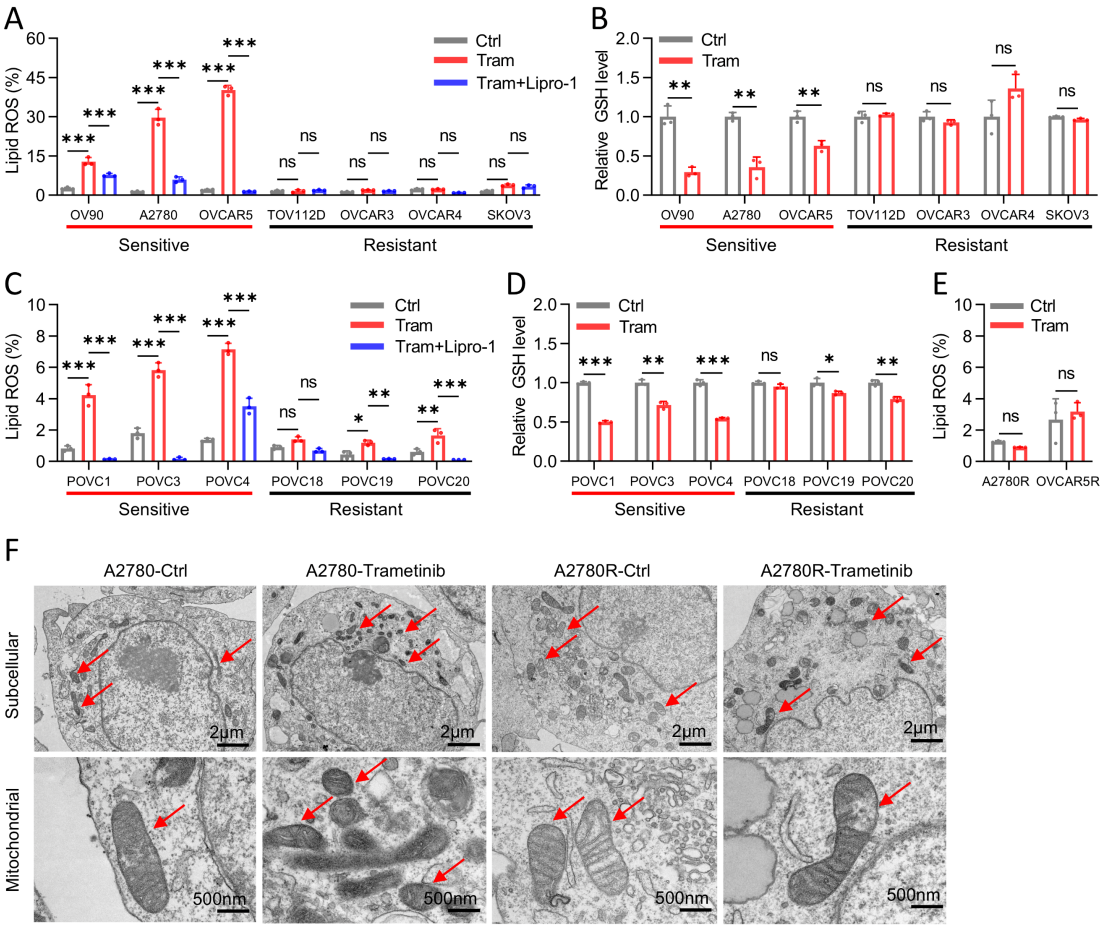
A
Lipid ROS (%)
Ctrl
Tram
Tram+Lipro-1
OV90
A2780
OVCAR5
TOV112D
OVCAR3
OVCAR4
SKOV3
Sensitive
Resistant
B
Relative GSH level
C
POVC1
POVC3
POVC4
POVC18
POVC19
POVC20
D
E
A2780R
OVCAR5R
F
A2780-Ctrl
A2780-Trametinib
A2780R-Ctrl
A2780R-Trametinib
Subcellular
Mitochondrial
2μm
500nm

Figure 2. Loss of ferroptosis is associated with the resistance to MEK inhibitors in OV. (A) Lipid ROS level and **(B)** intracellular GSH level of commercial OV cell lines with treated with trametinib (Tram, 200 nM) combined with or without Lipro-1 (100 nM). **(C)** Lipid ROS level and **(D)** intracellular GSH level of OV patient-derived cells (PDCs) treated with trametinib (200 nM) combined with or without Lipro-1 (100 nM). **(E)** Lipid peroxidation level of trametinib acquired-resistant cells A2780R and OVCAR5R treated with or without trametinib (200 nM). **(F)** A2780 and A2780R cells were treated with trametinib (200 nM) and analyzed by TEM to detect ultrastructure of mitochondria in two scale bars, 500 nm and 2 μm. The data are presented as the mean ± S.D. of three independent experiments. (A and C) P-values were determined by 1-way ANOVA with Bonferroni's post hoc test; (B, D and E) P- values were determined by unpaired Student's t test. ns, not significant, $*P < 0.05$, $**P < 0.01$, $***P < 0.001$.

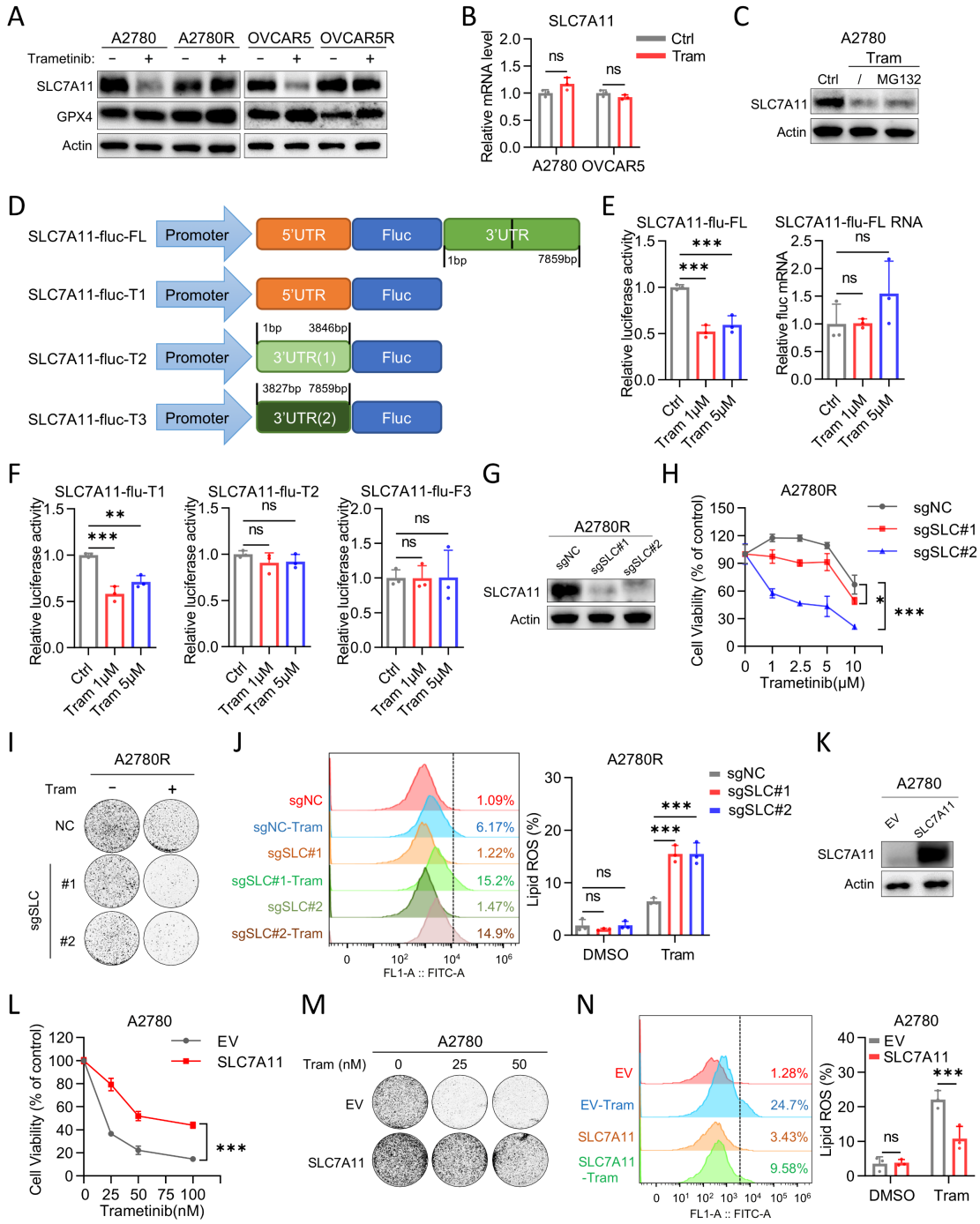

828

829 **Figure 3. SLC7A11 protein synthesis dictates the sensitivity of OV cells to**
830 **ferroptosis triggered by MEK inhibitors. (A)** Immunoblot analysis of SLC7A11 and
831 GPX4 in A2780 and OVCAR5 cells with their counterpart resistant lines treated with
832 trametinib (200 nM) for 48 hours. **(B)** qRT-PCR analysis of *SLC7A11* in A2780 and
833 OVCAR5 cells treated with trametinib (200 nM) for 48 hours. **(C)** Immunoblot analysis

of SLC7A11 in A2780 cell treated with trametinib (200 nM) for 48 hours followed by 1.0 μM MG132 for 6 hours before harvest. **(D)** Patterns of SLC7A11 luciferase reporter plasmids: SLC7A11-fluc-FL (promoter region, 5′-UTR, and 3′-UTR); SLC7A11-fluc-T1 (promoter region and 5′-UTR); SLC7A11-fluc-T2 (promoter region, 5′-UTR, and nt 1–3846 of 3′-UTR); and SLC7A11-fluc-T3 (promoter region, 5′-UTR, and nt 3827–7859 of 3′-UTR). **(E)** Relative luciferase activity of SLC7A11- FL and the mRNA level of SLC7A11-FL tested by qRT-PCR after SLC7A11-fluc-FL was transiently transfected into A2780 cells treated with trametinib for 48 hours. **(F)** Relative luciferase activity of SLC7A11-fluc-T1, SLC7A11-fluc-T2, and SLC7A11-fluc-T3 after transiently transfected into A2780 cell. In **E–F**, the relative luciferase activity was determined by calculating the ratio of firefly luciferase activity over renilla luciferase activity. Data are represented as mean ± SD, n = 3. **(G)** The effect of CRISPR/Cas9-mediated SLC7A11 knockdown (sgSLC#1 and sgSLC#2) evaluated by immunoblot analysis in A2780R. **(H)** Cell viability assay and **(I)** colony formation assay of the effect of SLC7A11 ablation and control (sgNC) on trametinib sensitivity in A2780R cells. The concentration of trametinib used in colony formation assay is 10μM. **(J)** BODIPY™ 581/591 C11 staining followed by cytometry analysis to investigate the effect of CRISPR/Cas9-mediated SLC7A11 knockdown on lipid peroxidation in A2780R under trametinib treatment (10μM). **(K)** The effect of SLC7A11 overexpression evaluated by immunoblot analysis in A2780. **(L)** Cell viability assay and **(M)** colony formation assay of empty vector (EV) and SLC7A11-overexpressing (SLC7A11) A2780 cells treated with trametinib at different concentrations. **(N)** Lipid peroxidation assay of A2780-EV and -SLC7A11 cells treated with trametinib (200nM). The data are presented as the mean ± S.D. of triple independent experiments. (B and N) P-values were determined by unpaired Student's t test. (E, F and J) P-values were determined by 1-way ANOVA with Bonferroni's post hoc test. (H and L) P-values were determined by 2-way ANOVA with Tukey's post hoc test. ns, not significant, $*P < 0.05$, $**P < 0.01$, $***P < 0.001$.

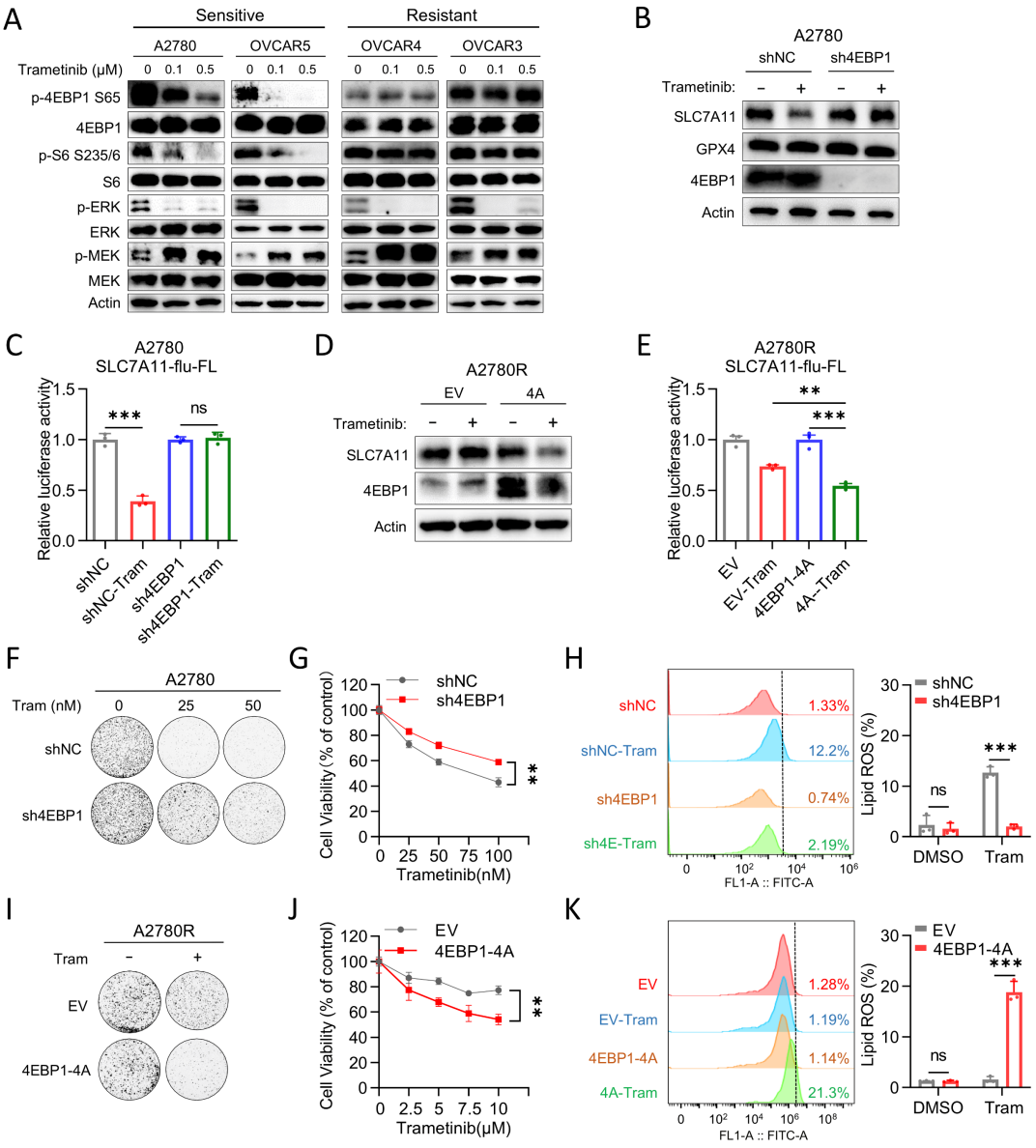
A
Sensitive
Resistant
A2780
OVCAR5
OVCAR4
OVCAR3
Trametinib (μM)
0 0.1 0.5
p-4EBP1 S65
4EBP1
p-S6 S235/6
S6
p-ERK
ERK
p-MEK
MEK
Actin
B
A2780
shNC
sh4EBP1
Trametinib:
SLC7A11
GPX4
4EBP1
Actin
C
A2780
SLC7A11-flu-FL
Relative luciferase activity
shNC
shNC-Tram
sh4EBP1
sh4EBP1-Tram
D
A2780R
EV
4A
E
A2780R
SLC7A11-flu-FL
EV
EV-Tram
4EBP1-4A
4A-Tram
F
A2780
Tram (nM)
G
Cell Viability (% of control)
Trametinib(nM)
H
FL1-A :: FITC-A
Lipid ROS (%)
DMSO
Tram
I
A2780R
Tram
J
Trametinib(μM)
K

Figure 4. mTOR-4EBP1 pathway modulates SLC7A11 protein synthesis to promote ferroptosis escape upon trametinib treatment.

(A) Immunoblot analysis of AKT, 4EBP1, S6 and ERK and MEK activity in A2780, OVCAR5, OVCAR3 and OVCAR4 cells treated with vehicle, 100 nM trametinib or 500nM trametinib. **(B)** Immunoblot analysis of SLC7A11, GPX4 and 4EBP1 in A2780 treated with trametinib (200nM) after transfection with either negative control (shNC) or sh4EBP1. **(C)** The relative luciferase activity of SLC7A11-flu-FL in A2780 treated with trametinib after transfection with either negative shNC or sh4EBP1. **(D)** Immunoblot analysis of SLC7A11, GPX4 and 4EBP1 in A2780R cells treated with trametinib (10μM) after stable expression of either EV or 4EBP1-4A. **(E)** The relative luciferase activity of SLC7A11-flu-FL in A2780R treated with trametinib after transfection with either EV or 4EBP1-4A. **(F)** Colony formation assay and **(G)** cell viability assay of the effect of 4EBP1 depletion on trametinib sensitivity. **(H)** The effect of 4EBP1 depletion on lipid peroxidation in A2780 treated with trametinib (200nM). **(I)** Colony formation assay and **(J)** cell viability assay of the effect of 4EBP1-4A overexpression on trametinib sensitivity (trametinib,10μM). **(K)** The effect of 4EBP1-4A overexpression on lipid peroxidation in A2780R treated with trametinib (10μM). The data are presented as the mean ± S.D. of three independent experiments. (C, H and K) P-values were determined by unpaired Student's t test. (E) P-values were determined by 1-way ANOVA with Bonferroni's post hoc test. (G and J) 2-way ANOVA with Tukey's post hoc test. ns, not significant, $^{**}P < 0.01$, $^{***}P < 0.001$.

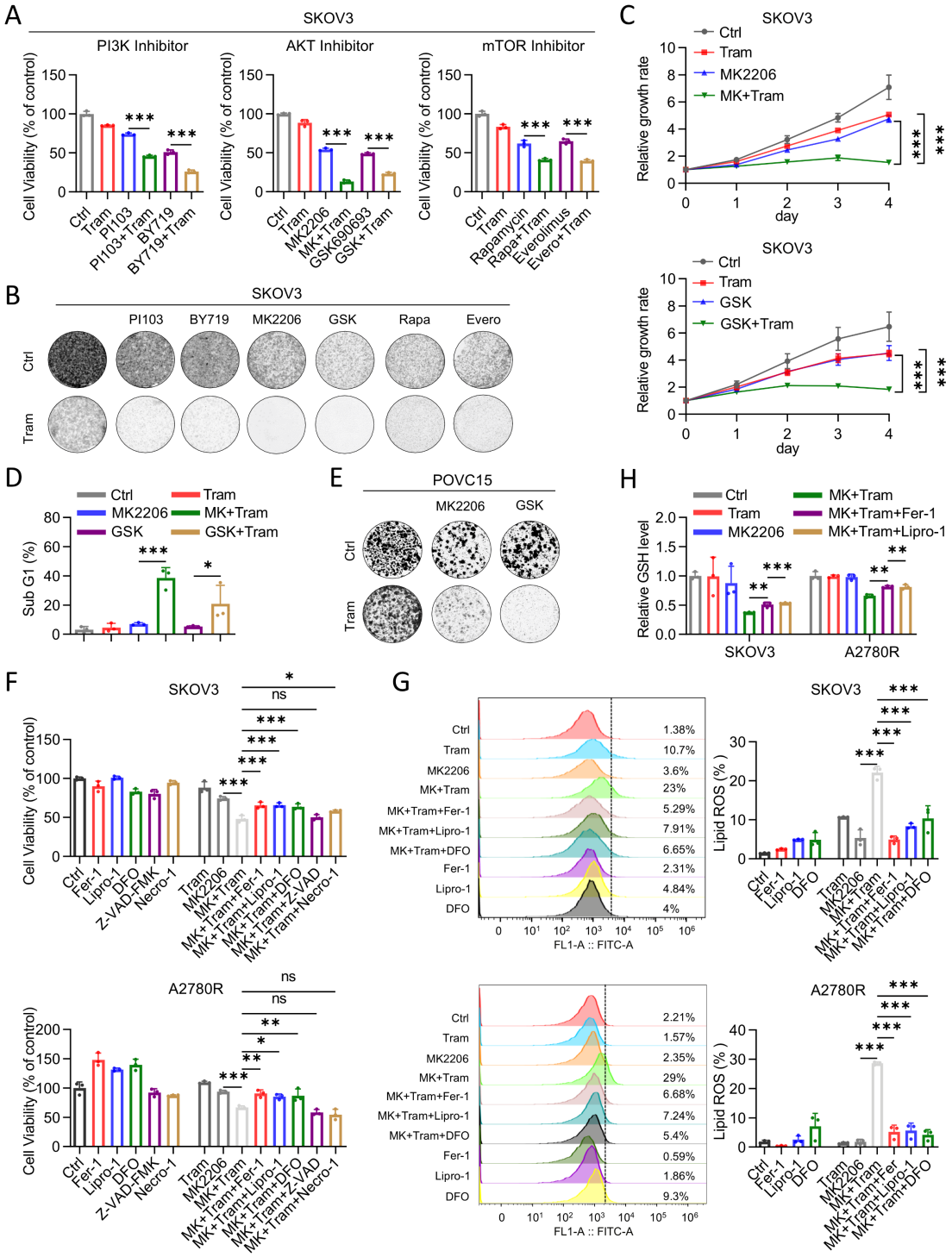
A
SKOV3
PI3K Inhibitor
AKT Inhibitor
mTOR Inhibitor
Cell Viability (% of control)
Ctrl
Tram
PI103
PI103+Tram
BY719
BY719+Tram
MK2206
MK+Tram
GSK690693
GSK+Tram
Rapamycin
Rapa+Tram
Everolimus
Evero+Tram
B
SKOV3
PI103
BY719
MK2206
GSK
Rapa
Evero
Ctrl
Tram
C
SKOV3
Relative growth rate
day
MK+Tram
GSK
GSK+Tram
D
Sub G1 (%)
MK2206
GSK
MK+Tram
GSK+Tram
E
POVC15
MK2206
GSK
H
Relative GSH level
MK+Tram+Fer-1
MK+Tram+Lipro-1
SKOV3
A2780R
F
Cell Viability (% of control)
Fer-1
Lipro-1
DFO
Z-VAD-FMK
Necro-1
MK+Tram+DFO
MK+Tram+Z-VAD
MK+Tram+Necro-1
G
FL1-A :: FITC-A
1.38%
10.7%
3.6%
23%
5.29%
7.91%
6.65%
2.31%
4.84%
4%
2.21%
1.57%
2.35%
29%
6.68%
7.24%
5.4%
0.59%
1.86%
9.3%
Lipid ROS (%)

Figure 5. Targeting PI3K/mTOR signaling sensitized resistant cells to ferroptosis induced by MEK inhibitors. (A) Cell viability of SKOV3 treated with 500nM trametinib with or without PI3K/AKT/mTOR inhibitors for 96 hours. BY719 (1μM), PI103 (1μM), MK2206 (MK) (5μM), GSK690693 (GSK) (5μM), Rapamycin (Rapa) (1μM), Everolimus (Evero) (0.5μM). **(B)** Colony formation of SKOV3 treated with 500nM trametinib with or without PI3K/AKT/mTOR inhibitors. BY719 (1μM), PI103 (1μM), MK2206 (MK) (5μM), GSK690693 (GSK) (5μM), Rapamycin (Rapa) (1μM), Everolimus (Evero) (0.5μM). **(C)** Growth curves and (**D)** Sub-G1 population analysis in SKOV3 treated with either vehicle, trametinib, AKT inhibitors (GSK690693 or MK2206) or their combination. **(E)** Colony formation assay of PDC-POVC15 treated with trametinib (100 nM) with or without AKT inhibitors (MK2206, 5μM and GSK690693, 5μM). **(F)** Cell viability of SKOV3 and A2780R cells following trametinib (500nM) and/ or MK2206 treatment (5μM) in the presence or absence of Fer-1 (2μM), Lipro-1 (100nM), DFO (300nM), Z-VAD (5 μM) and Necro-1 (5 μM) for 48 hours. MT: MK2206 combined with Trametinib **(G)** Detection of lipid peroxidation level with BODIPYTM 581/591 C11 probe determined by the flow cytometer in SKOV3 and A2780R treated with trametinib (500 nM) and/ or MK2206 (5μM) treatment in the presence or absence of Fer-1, Lipro-1 and DFO for 48 hours. **(H)** Detection of GSH level in SKOV3 and A2780R followed by trametinib (500 nM) and/ or MK2206 treatment (5μM) in the presence or absence of Fer-1 or Lipro-1 for 48 hours. The data are presented as the mean ± S.D. of three independent experiments. (A, F, G and H) P-values were determined by 1-way ANOVA with Bonferroni's post hoc test. (C) P-values were determined by 2-way ANOVA with Tukey's post hoc test. ns, not significant. (D) P-values were determined by unpaired Student's t test. $*P < 0.05$, $**P < 0.01$, $***P < 0.001$.

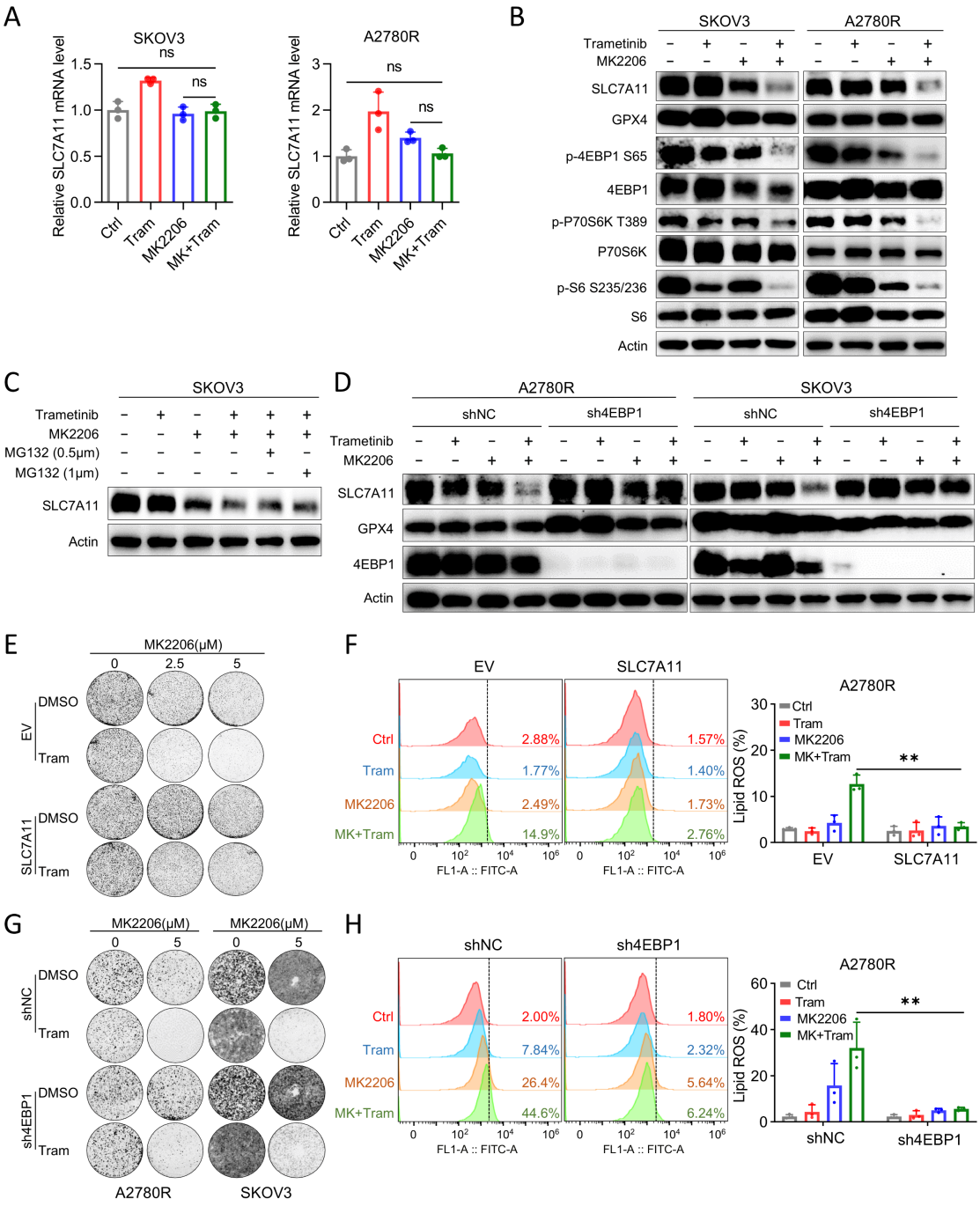
A
SKOV3
A2780R
Relative SLC7A11 mRNA level
ns
Ctrl
Tram
MK2206
MK+Tram
B
Trametinib
MK2206
SLC7A11
GPX4
p-4EBP1 S65
4EBP1
p-P70S6K T389
P70S6K
p-S6 S235/236
S6
Actin
C
MG132 (0.5μm)
MG132 (1μm)
D
shNC
sh4EBP1
E
MK2206(μM)
DMSO
EV
SLC7A11
Tram
F
EV
SLC7A11
Lipid ROS (%)
FL1-A :: FITC-A
G
shNC
sh4EBP1
H

Figure 6. Co-targeting AKT and MEK suppresses the protein synthesis of SLC7A11 via inhibition of mTOR-4EBP1 activity. (A) The mRNA level of SLC7A11 in SKOV3 and A2780R treated with vehicle, trametinib (500 nM), MK2206 (5μM) or their combination for 48 hours. **(B)** Immunoblot analysis of SLC7A11, GPX4 and the activity of mTOR, 4EBP1, P70S6K and S6 in SKOV3 and A2780R cells treated with vehicle, trametinib (500 nM), MK2206 (5μM) or their combination for 48 hours. **(C)** Immunoblot analysis of SLC7A11 in SKOV3 treated with trametinib and/ or MK2206 treatment for 48 hours in the presence or absence of MG132 at indicated concentrations for 6 hours before harvest**. (D)** Immunoblot analysis of SLC7A11 in SKOV3 and A2780R treated with trametinib (500 nM) and/ or MK2206 (5μM) after transfection with either shNC or sh4EBP1 for 48 hours. **(E)** Representative images of colony formation assay in A2780R cells treated with trametinib (500 nM) with or without MK2206 (both 2.5μM and 5μM) after transfection with either EV or SLC7A11. **(F)** Lipid peroxidation analysis in A2780R cells treated with trametinib (500 nM) with or without MK2206 (5μM) for 48 hours after transfection with either EV or SLC7A11. **(G)** Representative images of colony formation assay in A2780R and SKOV3 cells treated with trametinib (500 nM) with or without MK2206 (5μM) after transfection with either shNC or sh4EBP1. **(H)** Lipid peroxidation analysis in A2780R cells treated with trametinib (500 nM) with or without MK2206 (5μM) for 48 hours after transfection with either shNC or sh4EBP1. The data are presented as the mean ± S.D. of three independent experiments. (A) P-values were determined by 1-way ANOVA with Bonferroni's post hoc test. (F and H) P-values were determined by unpaired Student's t test. ns, not significant, $^{**}P < 0.01$.

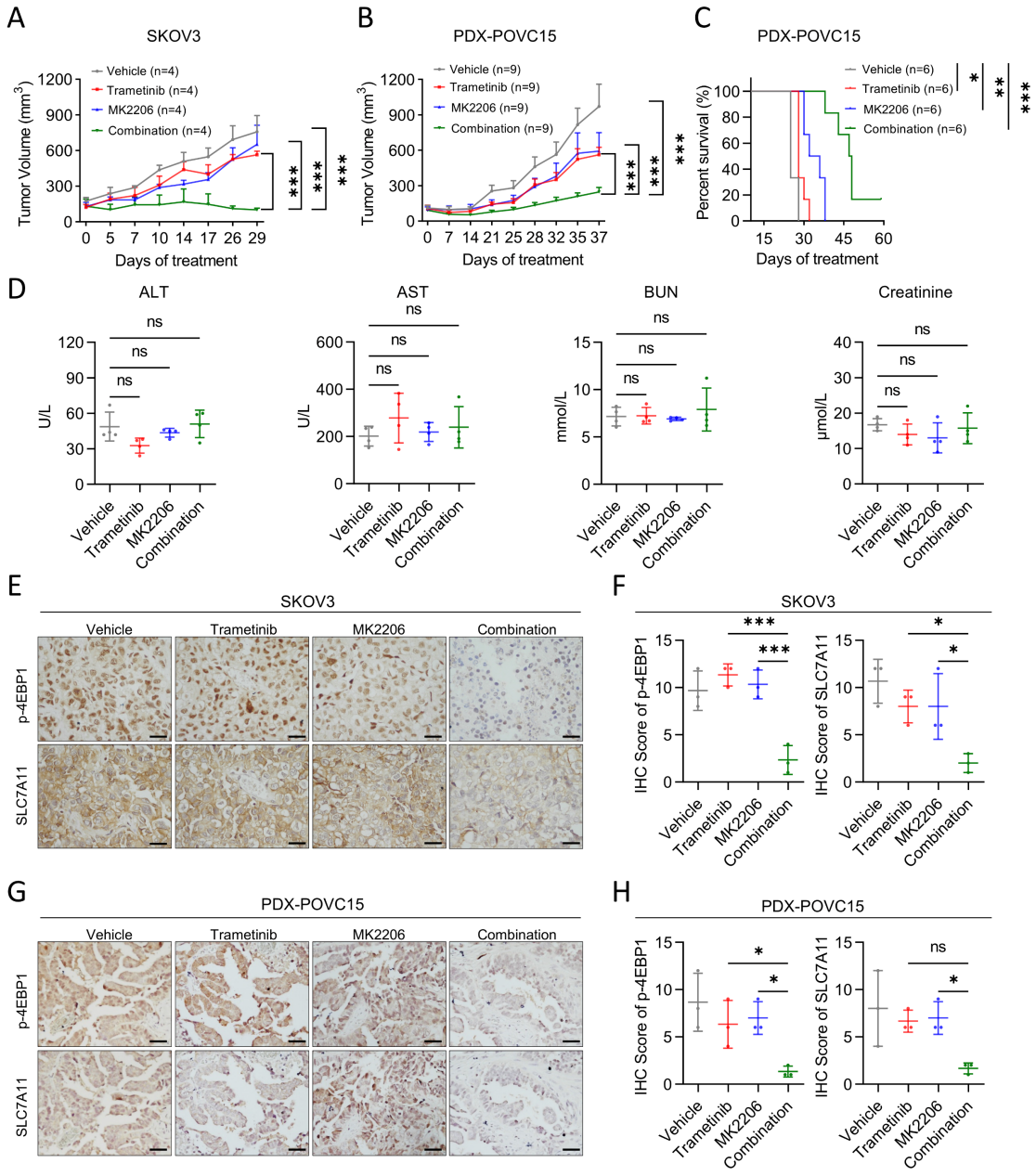
A
SKOV3
Vehicle (n=4)
Trametinib (n=4)
MK2206 (n=4)
Combination (n=4)
Tumor Volume (mm3)
Days of treatment
B
PDX-POVC15
Vehicle (n=9)
Trametinib (n=9)
MK2206 (n=9)
Combination (n=9)
Tumor Volume (mm3)
Days of treatment
C
PDX-POVC15
Vehicle (n=6)
Trametinib (n=6)
MK2206 (n=6)
Combination (n=6)
Percent survival (%)
Days of treatment
D
ALT
AST
BUN
Creatinine
U/L
mmol/L
μmol/L
ns
Vehicle
Trametinib
MK2206
Combination
E
SKOV3
Vehicle
Trametinib
MK2206
Combination
p-4EBP1
SLC7A11
F
SKOV3
IHC Score of p-4EBP1
IHC Score of SLC7A11
G
PDX-POVC15
H
PDX-POVC15

Figure 7. AKT inhibitor sensitizes OV to MEK inhibitor-mediated ferroptosis *in vivo*. (A) Tumor volume of SKOV3 xenografts in nude mice treated with vehicle, 60 mg/kg MK2206 (orally), 0.25 mg/kg trametinib (i.p.) or the combination at the same doses every other day (n = 4 per group). **(B)** Tumor volume of patient-derived xenograft PDX-POVC15 tumors implanted into NOD-SCID mice treated with vehicle, 90 mg/kg MK2206 (orally), 0.25 mg/kg trametinib (i.p.) or the combination at the same doses every other day (n = 9 per group). **(C)** Survival rates of patient-derived xenograft PDX-POVC15 tumors implanted into NOD-SCID mice treated with vehicle, 90 mg/kg MK2206 (orally), 0.25 mg/kg trametinib (i.p.) or the combination at the same doses every other day (n = 6 per group)**.** The curve represents the survival time from the beginning of therapy. Drug treatment was withdrawn until the tumor volume of the first mouse reached 1000 mm^3 at day 25. **(D)** Quantification of alanine aminotransferase (ALT), aspartate aminotransferase (AST), BUN and creatinine levels in the serum of PDX-POVC15 of experiments described in (C**)** at day 25 (n = 4 per group). **(E)** Representative IHC and **(F)** quantification of p-4EBP1 and SLC7A11 in SKOV3 of experiments described in **A**. Scale bar, 50 μm. **(G)** Representative IHC and **(H)** quantification of p-4EBP1 and SLC7A11 in PDX-POVC15 of experiments described in (B). Scale bar, 100 μm. (A–C) Date are presented as mean ± SEM. P-values were determined by two-way ANOVA with Tukey's post hoc test. (D, F and H) Quantification is shown from 3 tumors. The data are presented as the mean ± S.D. P-values were determined by 1-way ANOVA with Bonferroni's post hoc test. ns, not significant, $*P < 0.05$, $**P < 0.01$, $***P < 0.001$.

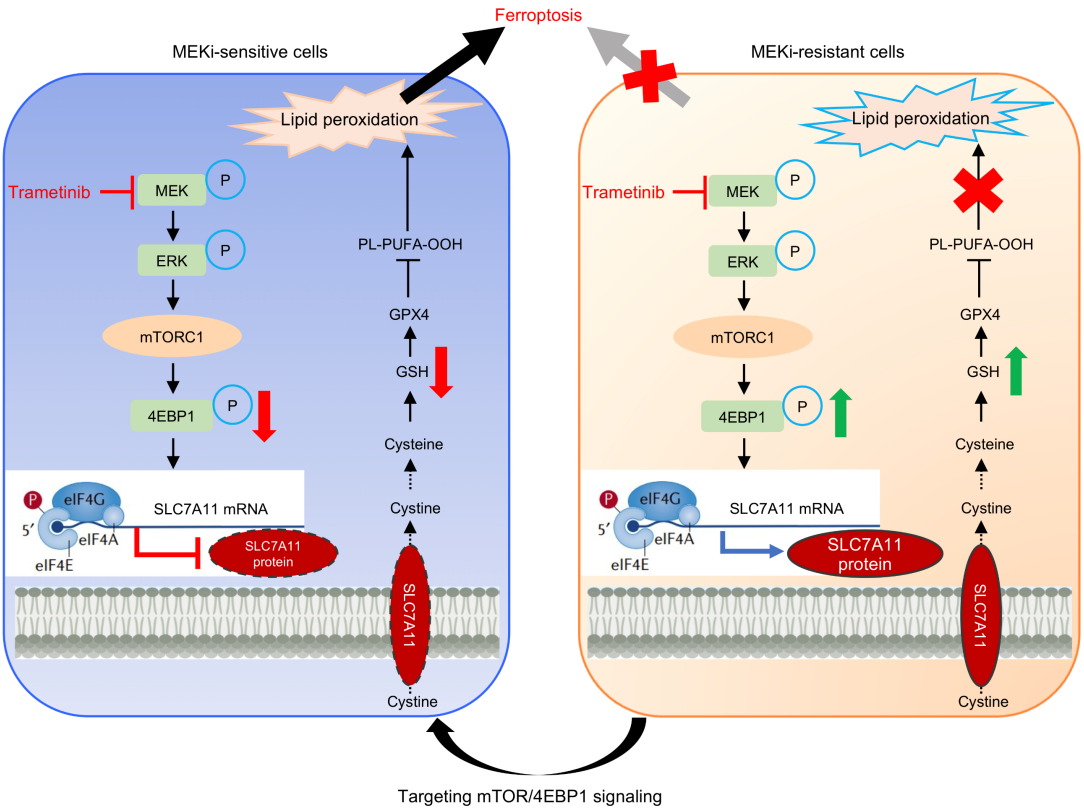

978

979 **Figure 8. The schematic model illustrating the mechanism of ferroptosis**
980 **modulated by MEK inhibitor.**

981 Trametinib inhibits mTOR/4EBP1 activity to suppress SLC7A11 protein synthesis,
982 leading to ferroptosis in MEK inhibitor sensitive OV cells **(Left)**. Sustained mTOR-
983 4EBP1 axis mediated SLC7A11 translation and conferred resistance to trametinib-
984 induced ferroptosis (**Right**). Targeting mTOR/4EBP1 signaling reversed the resistance
985 to ferroptosis induced by MEK inhibitors through suppression of SLC7A11 protein
986 synthesis.